A two-dimensional isogeometric boundary element method for linear elastic fracture

X. Peng[1], E. Atroshchenko[2], S. Kulasegaram[1], S. P. A. Bordas[1,3]¶

[1]Institute of Mechanics and Advanced materials, Cardiff University, CF24 3AA, UK

[2]Department of Mechanical Engineering, University of Chile, Santiago, 8370448, Chile

[3]Université du Luxembourg, Faculté des Sciences, de la Technologie et de la Communication, 6, rue Richard Coudenhove-Kalergi, L-1359 Luxembourg – Research Unit in Engineering Science Campus Kirchberg, G 007

ABSTRACT

The present work proposes a method for simulating linear elastic fracture and crack growth through an isogeometric boundary element method. Non-Uniform Rational B-Splines (NURBS) are used to approximate the geometry, boundary displacements and boundary tractions. Collocation is employed to generate the system of equations. To avoid the degeneration of the system matrix seen when modelling coincident crack surfaces with conventional boundary element methods, a dual boundary element method formulation, which makes use of two independent boundary integral equations, is applied. To capture the stress singularity around the crack tip in the framework of linear elastic fracture mechanics, two methods are proposed: (1) a graded knot insertion near crack tip; (2) partition of unity enrichment. A well-established CAD algorithm is adopted to generate a smooth crack surface as the crack grows. The M integral and J_k integral methods for the extraction of stress intensity factors are compared in terms of accuracy and efficiency. The numerical results are compared against closed-form solutions as well as other numerical methods, namely the collocation BEM with a Lagrangian basis, a symmetric Galerkin BEM and extended finite element methods. The crack growth paths obtained by the proposed method are validated using experimental data.

Key Words: *Isogeometric analysis; NURBS; Linear elastic fracture; Boundary element method; Crack growth.*

¶Corresponding author. Tel:(+352)4666445567 Fax:(+352)46664435567
E-mail address:stephane.bordas@alum.northwestern.edu

1 Introduction

The efficiency of the boundary element method (BEM) in modeling fracture problems is based on two reasons: (1) due to the integral representation of solutions inside the domain, the accuracy of the BEM in capturing the stress concentration or singularity is higher in comparison with domain integration methods like the finite element method (FEM); (2) the dimensionality of the problem in BEM is reduced by one in comparison with domain-type methods like FEM and only the change of the boundary needs to be taken into account when crack evolves, which greatly releases the computational burden and simplifies the remeshing procedure. The important issue for modeling fracture using BEM is the degeneration of the system matrix when the source points are placed on the overlapped crack surfaces. Many works have been proposed to address this problem. Blandford *et al* [1] used the multi-region method to model crack problems by dividing the domain into sub-domains along the crack surface and introducing artificial-created boundaries. This approach is cumbersome in dealing with multiple cracks and crack propagation problems. Synder and Cruse [2] developed a modified fundamental kernel for infinite domain containing flat, traction free crack and it works well for 2D mixed-mode crack. However, it is hard to extend this work to the general scenarios of the crack modeling. The most popular approach to overcome the degeneration of the system is to to prescribe displacement boundary integral equation (BIE) on one crack surface and traction BIE on the other crack surface. The method is called dual boundary element method (DBEM) [3]. DBEM provides an efficient way to model cracks of arbitrary 1D and 2D geometries [4][5][6][7]. Another way to model crack problems is named displacement discontinuity method (DDM) [8], which is mostly suitable for problems with symmetry. In this method, the two overlapped crack surfaces are replaced by one of the surface, which drastically decreases the computational model size. And the displacement and traction discontinuities on the crack surface are used as primary quantities instead of displacement and traction on the two crack surfaces in DBEM. in such case, even a single traction BIE can be used for fracture problems [9]. DDM is proved to be a special formation of DBEM later by Partheymüller *et al* [10], and they extended the application of DDM from symmetric loaded cracks to asymmetric loaded cracks. However the displacement is indirect on the crack surface since only displacement discontinuity is obtained. Additional postprocess needs to be done to retrieve the displacement solution which increases

the computational burden. Another branch of work focuses on the Galerkin formulation of BEM, particularly symmetric Galerkin BEM (SGBEM), for fracture mechanics, which primarily based on DDM [11][12][13]. In Galerkin formulation, the error estimation theory is well developed and the boundary continuity requirement is relaxed to be C^0 for hypersingular BIE due to the application of weak form [14]. However, double integrals need to be evaluated which makes it much slower then the traditional collocation BEM. In order to make the crack modeling more efficient for large scale problems, some BEM-FEM coupled schemes are proposed [15][16][17]. The general idea is to subdivide the cracked domain into two sub-domains, the BEM sub-domain and the FEM sub-domain, to take advantage of both methods. Some other methods like boundary element-free method, which is based on moving least square approximation, is also proposed and applied to fracture modeling [18].

The accurate evaluation of stress intensity factors (SIFs) plays a pivot role for crack growth modeling. Nevertheless, due to the $1/\sqrt{r}$ stress singularity in the vicinity of the crack tip, special care should be taken in the numerical methods in order to obtain a more accurate and reliable SIFs. One of the ways to capture the asymptotics of the displacement and stress fields in the vicinity of a crack is by means of special crack tip elements. For example, so called quarter-point element, where the middle nodes are shifted to the positions of one quarter of the element sides from the crack edge [19][20]. This modification results in the exact representation of the $1/\sqrt{r}$ singularity in the near-tip stress field and allows to extract SIF directly [21]. Another example is the hybrid crack element, developed in both FEM and BEM communities [22][23], which introduces the the asymptotic behavior of the stress field around crack tip in to the tip-element so that the SIFs can be output directly and accurately.

The partition-of-unity based enrichment idea [24] is widely used to capture the singularity near the crack tip in linear elastic fracture mechanics. The popular extended finite element method (XFEM) [25], extended meshfree method [26] has been widely investigated for both 2D and 3D fracture propagation problems. The enriched stress field can result in a much more accurate SIFs than the classical one. And the enrichment idea has been introduced in BEM as well [18][27][28]. The virtual crack closure technique (VCCT) based on the Irwin's integral of strain energy release rates, is another common method to extract SIFs in FEM and BEM, and recently has been extended to XFEM and extended element-free Galerkin method (XEFG) [29][30]. Since the near-tip singular behavior is already known as Williams solution, the idea to

remove the singularity is proposed and the SIFs can be output directly as well [31]. However, the Williams solution is only valid in the near-tip region. The near-tip region is ambiguous in practical problems. The J integral based methods are regarded as very accurate approaches to extract SIFs in both FEM and BEM communities. Different kinds of extraction from J_1 (J) are developed, such as the symmetric and asymmetric decomposition of J_1 [32], the M integral (interaction energy integral) [33]. Chang and Wu [34] proposed the J_k method which does not need to introduce any auxiliary fields and suitable for no matter flat and curved cracks. We note that in the implementation of FEM/XFEM and other domain type methods, these contour integrals are always cast into domain integrals since the FEM-solution and the related quantities are obtained inside the domain [35][36][25]. However, in BEM it is easier to deal with the contour integrals, since obtaining solutions inside the domain requires additional integration, while evaluating J_k, M - integrals along the crack surfaces is done directly and straightforwardly due to the boundary nature of BEM-solutions. The later two contour integral methods, namely J_k and M - integrals are discussed in detail in this paper.

The isogeometric analysis (IGA)[37] has been proposed as an alternative fundamental methodology to the traditional Lagrange polynomial based analyses. The IGA utilizes the same splines, that are used to exactly represent the geometry, as the basis function for the approximation of the unknown fields, which builds up a more direct link between CAD and analysis. The non-uniform rational B-splines (NURBS) based IGA has been widely investigated in many areas [38][39][40][41][42]. Another, more flexible geometrical representation technique named T-spline has been introduced to overcome the difficulties presented in NURBS, such as [43][44]. Recently the IGA has been incorporated with BEM and applied in exterior potential-flow problems [45], potential problems [46], elastostatics [47][48], shape optimization [49], Stokes flow [50] and acoustic [28][51] etc. The isogeometric BEM (IGABEM) presents another way for isogeometric analysis due to the natural fit between the two methods. Currently, the dominated CAD geometry only provides surface description by smooth splines. This is in consistence with the basic feature of the BEM since only the unknown fields (displacement and traction) along the boundary is required to approximate. And the convergence rule of collocation BEM with splines has been investigated earlier which forms the solid theoretical basis of the combined methodology [52][53]. In this paper, a new application of IGABEM is discussed in detail for linear elastic fracture problems. It should be noted that knot insertion in B-splines can introduce

discontinuities in the geometry, which makes it possible to extend IGA into the application for fracture mechanics [54]. The higher order continuity provided by splines also enables a more straightforward way to introduce traction BIE for crack modeling. This paper presents a basic scheme for the fracture modeling and crack propagation for 2D domain.

The paper is organized as follows: The concept of NURBS basis is reviewed shortly in section 2. The basic idea of DBEM for fracture modeling is briefly reviewed in section 3, and more details are followed involving collocation and singular integration in DBEM. Section 4 concludes the approaches for extraction of the SIFs, based on M integral and J_k integral. section 5 outlines a modifying-NURBS approach to simulate crack growth using NURBS based representation for cracks. Numerical examples are shown both for fracture analysis and crack propagation, in comparison with other popular methods like SGBEM, XFEM and XEFG.

2 NURBS basis functions

The NURBS basis functions are the generalization of B-spline functions that allows a "projection" to form complex geometries. So the basic concept of B-spline is first outlined here. B-spline basis functions are defined over the knot vector, which is a non-decreased sequence of real numbers given in the parameter space. A knot vector is denoted as $\Xi = \{\xi_1, \xi_2, ..., \xi_{n+p+1}\}$, where $\xi_A \in \mathbb{R}$ is the A^{th} parameter coordinate (knot), p is the order of the polynomial in B-spline basis functions, n is the number of the basis functions. For a given order p, the B-spline basis functions $N_{A,p}$ with $1 \leqslant a \leqslant n$ are defined by the Cox-de Boor recursion:

$$N_{A,0}(\xi) = \begin{cases} 1 & \xi_A \leqslant \xi < \xi_{A+1} \\ 0 & \text{otherwise,} \end{cases} \tag{1}$$

then, for $p > 0$,

$$N_{A,p}(\xi) = \frac{\xi - \xi_A}{\xi_{A+p} - \xi_A} N_{A,p-1}(\xi) + \frac{\xi_{A+p+1} - \xi}{\xi_{A+p+1} - \xi_{A+1}} N_{A+1,p-1}(\xi). \tag{2}$$

The continuity of B-spline basis functions at ξ_A can be decreased by repeating the knot several times. If ξ_A has multiplicity k ($\xi_A = \xi_{A+1} = ... = \xi_{A+k-1}$), then the basis functions are C^{p-k} continuous at ξ_A. Particularly, when $k = p$, the basis is C^0 and $k = p + 1$ leading to a

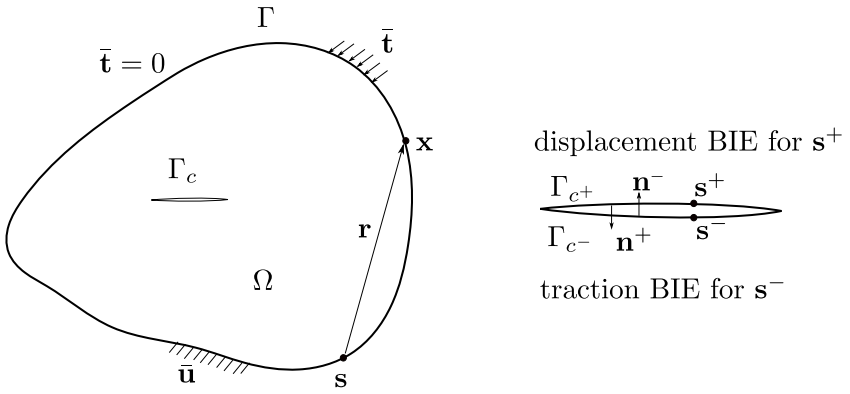

(a) (b)

Figure 1: Crack model

discontinuity at ξ_A. If the fist and last knot have $k = p + 1$, the knot vector is called an open knot vector. More details can be referred in [55].

Having defined the B-spline basis functions $\mathbf{N} = \{N_{A,p}\}_{A=1}^{n}$, we can describe a curve $C(\xi)$ in $\mathbb{R}^{d_s}$ (d_s is the spatial dimensionality, $d_s = 2$ in this paper) by a group of control points $\mathbf{P} = \{\mathbf{P}_A\}_{A=1}^{n}$ with them as:

$$C(\xi) = \sum_{A=1}^{n} P_A N_{A,p}(\xi) \tag{3}$$

The NURBS curve is defined in the same way except replacing the B-spline basis functions into NURBS basis functions. For example, a NURBS curve $C(\xi)$ can be described as:

$$C(\xi) = \sum_{A=1}^{n} P_A R_{A,p}(\xi) \tag{4}$$

where $R_{A,p}$ are the NURBS basis functions, which are defined as;

$$R_{A,p}(\xi) = \frac{\omega_A N_{A,p}(\xi)}{\sum_{B=1}^{n} \omega_B N_{B,p}(\xi)}. \tag{5}$$

ω_B is the weight associated with the B^{th} control point. Note that $R_{A,p}$ is only non-zero on the knot interval $[\xi_a, \xi_b]$) defined by $p + 1$ control points.

3 Isogeometric DBEM for frature modeling

3.1 Problem formulation

Consider an arbitrary domain Ω which contains a crack as in Figure 1. The boundary Γ is composed of Γ_u where Dirichlet boundary condition is prescribed with known displacement $\bar{\mathbf{u}}$, Γ_t where Neumann boundary condition is prescribed with known traction $\bar{\mathbf{t}}$. All the remaining part is defaulted as traction-free boundary $\bar{\mathbf{t}} = 0$ with the unknown displacement. The crack Γ_c is composed of two coincident faces: Γ_{c^+} and Γ_{c^-} and traction-free crack problem is assumed in this work. $\mathbf{s} = (s_1, s_2)$ denotes the source point and $\mathbf{x} = (x_1, x_2)$ the field point. The displacement BIE at the source point $\mathbf{s}$ is given by

$$c_{ij}(\mathbf{s})u_j(\mathbf{s}) + \int\!\!\!\!\!\!-_{\Gamma} T_{ij}(\mathbf{s},\mathbf{x})u_j(\mathbf{x})\mathrm{d}\Gamma(\mathbf{x}) = \int_{\Gamma} U_{ij}(\mathbf{s},\mathbf{x})t_j(\mathbf{x})\mathrm{d}\Gamma(\mathbf{x}) \tag{6}$$

where the U_{ij}, T_{ij} are called fundamental solutions, given by

$$U_{ij}(\mathbf{s},\mathbf{x}) = \frac{1}{8\pi\mu(1-\nu)}\left[(3-4\nu)\delta_{ij}\ln\left(\frac{1}{r}\right) + r_{,i}r_{,j}\right] \tag{7}$$

$$T_{ij}(\mathbf{s},\mathbf{x}) = \frac{1}{4\pi\mu(1-\nu)r}\left\{\frac{\partial r}{\partial n}[(1-2\nu)\delta_{ij} + 2r_{,i}r_{,j}] - (1-2\nu)(r_{,i}n_j - r_{,j}n_i)\right\} \tag{8}$$

for $2D$ under plane strain condition, where $\mu = E/[2(1+\nu)]$, E the Young's Modulus, ν the Poisson's ratio. Components T_{ij} exhibit a singularity of $O(1/r)$ and the sign $\int\!\!\!\!\!\!-$ implies that the corresponding integrals are understood in the sense of Cauchy Principal Value (CPV), $|\mathbf{r}| = |\mathbf{x} - \mathbf{s}|$. and U_{ij} is weakly-singular (of order $O(\ln(1/r))$).

The idea of the boundary element method is to discretize the boundary geometry and the physical fields using sets of basis functions. Subsequently, the source point is placed at the collocation points and the displacement BIE (6) is transformed into the system of linear algebraic equations. However, when the domain contains a crack, the collocation points on the overlapped surfaces refer to the Figure 1 (b), Γ_{c^+} coincide with Γ_{c^-} and the system matrix becomes singular. This difficulty is overcome in dual boundary element method by prescribing traction BIE on one of the crack faces (Γ_{c^-} in Figure 1(b)), and displacement BIE on the other crack surface (Γ_{c^+}) and the rest of the boundary Γ. The traction BIE is obtained by differentiation of displacement

BIE with respect to $\mathbf{s}$ and multiplying the elastic tensor E_{ijkl}:

$$c_{ij}(\mathbf{s})t_j(\mathbf{s}) + \fint_\Gamma S_{ij}(\mathbf{s},\mathbf{x})u_j(\mathbf{x})\mathrm{d}\Gamma(\mathbf{x}) = \int_\Gamma K_{ij}(\mathbf{s},\mathbf{x})t_j(\mathbf{x})\mathrm{d}\Gamma(\mathbf{x}) \tag{9}$$

$$S_{ij}(\mathbf{s},\mathbf{x}) = E_{ikpq}\frac{\partial T_{pj}(\mathbf{s},\mathbf{x})}{\partial s_q}n_k(\mathbf{s}), \quad K_{ij}(\mathbf{s},\mathbf{x}) = E_{ikpq}\frac{\partial U_{pj}(\mathbf{s},\mathbf{x})}{\partial s_q}n_k(\mathbf{s}) \tag{10}$$

where S_{ij} is the hypersingular kernel ($O(1/r^2)$) and the sign $\fint$ denotes the Hadamard finite part integrals and K_{ij} is of order $O(1/r)$. The fundermental solutions for traction BIE are detailed in the Appendix A. $c_{ij}(\mathbf{s}) = 0.5\delta_{ij}$ when the source point $\mathbf{s}$ is on the smooth boundary.

3.2 NURBS discretisation

In the NURBS based isogeometric concept, The physical field is approximated by the same NURBS basis functions which are used to describe the geometry $\Gamma = C(\xi)$. The displacement and traction can be approximated as following:

$$u_i(\xi) = \sum_{A=1}^{n} R_{A,p}(\xi)d_i^A \tag{11}$$

$$t_i(\xi) = \sum_{A=1}^{n} R_{A,p}(\xi)q_i^A \tag{12}$$

We define an element in the parameter space as an interval between two consequent non-repeated knots $[\xi_a, \xi_b]$ and linearly transform it on interval $[-1, 1]$, which is called "parent space" [37]. We define $\hat{\xi}$ as the parent coordinate of the field point $\mathbf{x}$ in $[-1, 1]$, $\hat{\xi}_s$ as the parent coordinate of the source point $\mathbf{s}$ in $[-1, 1]$, and $J(\hat{\xi})$ is the Jacobian transformation from physical space to parent space. The transformation process for one NURBS element (the knot interval $[\xi_a, \xi_b]$) to the parent space $[-1, 1]$ is shown in Figure 2. And we have

$$\begin{aligned} \xi = \xi(\hat{\xi}) &= \frac{(\xi_b - \xi_a)\hat{\xi} + (\xi_b + \xi_a)}{2}, \\ J(\hat{\xi}) &= \frac{\mathrm{d}\Gamma}{\mathrm{d}\xi}\frac{\mathrm{d}\xi}{\mathrm{d}\hat{\xi}} \end{aligned} \tag{13}$$

Then above form can also be written via the elemental approximation as:

$$u_i(\hat{\xi}) = \sum_{I=1}^{p+1} N_I(\hat{\xi})d_i^I \tag{14}$$

$$t_i(\hat{\xi}) = \sum_{I=1}^{p+1} N_I(\hat{\xi}) q_i^I \tag{15}$$

where

$$N_I(\hat{\xi}) = R_{A,p}(\xi) \tag{16}$$

And d_i, q_i are displacement and traction control variables respectively. The relation of local index I and global index A is given by the element connectivity [47]. Substituting the discretized displacements and tractions into the BIEs will give,

$$\sum_{I}^{p+1} C_{ij}^I(\mathbf{s}) d_j^I + \sum_{e=1}^{N_e} \sum_{I}^{p+1} T_{ij}^I d_j^I = \sum_{e=1}^{N_e} \sum_{I}^{p+1} U_{ij}^I q_j^I \tag{17}$$

$$\sum_{I}^{p+1} C_{ij}^I(\mathbf{s}) t_j^I + \sum_{e=1}^{N_e} \sum_{I}^{p+1} S_{ij}^I d_j^I = \sum_{e=1}^{N_e} \sum_{I}^{p+1} K_{ij}^I q_j^I \tag{18}$$

where the the jump term and integrals of the fundamental solutions are respectively as:

$$C_{ij}^I(\mathbf{s}) = c_{ij} N_I(\hat{\xi}_s) \tag{19}$$

$$T_{ij}^I = \int_{-1}^{1} T_{ij}(\mathbf{s}, \mathbf{x}(\hat{\xi})) N_I(\hat{\xi}) J(\hat{\xi}) \mathrm{d}\hat{\xi} \tag{20}$$

$$U_{ij}^I = \int_{-1}^{1} U_{ij}(\mathbf{s}, \mathbf{x}(\hat{\xi})) N_I(\hat{\xi}) J(\hat{\xi}) \mathrm{d}\hat{\xi} \tag{21}$$

$$S_{ij}^I = \int_{-1}^{1} S_{ij}(\mathbf{s}, \mathbf{x}(\hat{\xi})) N_I(\hat{\xi}) J(\hat{\xi}) \mathrm{d}\hat{\xi} \tag{22}$$

$$K_{ij}^I = \int_{-1}^{1} K_{ij}(\mathbf{s}, \mathbf{x}(\hat{\xi})) N_I(\hat{\xi}) J(\hat{\xi}) \mathrm{d}\hat{\xi} \tag{23}$$

3.3 Treatment of singular integrals

Integration of weakly-singular, strongly-singular and hyper-singular kernels in Equations (20)-(23) presents a major difficulty in BEM. In present work, weakly-singular integrals are evaluated using Telles transformation [56]. Strongly-singular integrals in Equation (6) are treated in two different ways. In the first approach, the singularity in T_{ij} is removed by the regularization method, based on use of "simple solutions" [57][58], i.e. the rigid body motions, which satisfy Equation (6) with zero tractions. Adding and subtracting term $\mathbf{u}(\mathbf{s})$ in Equation (6), the

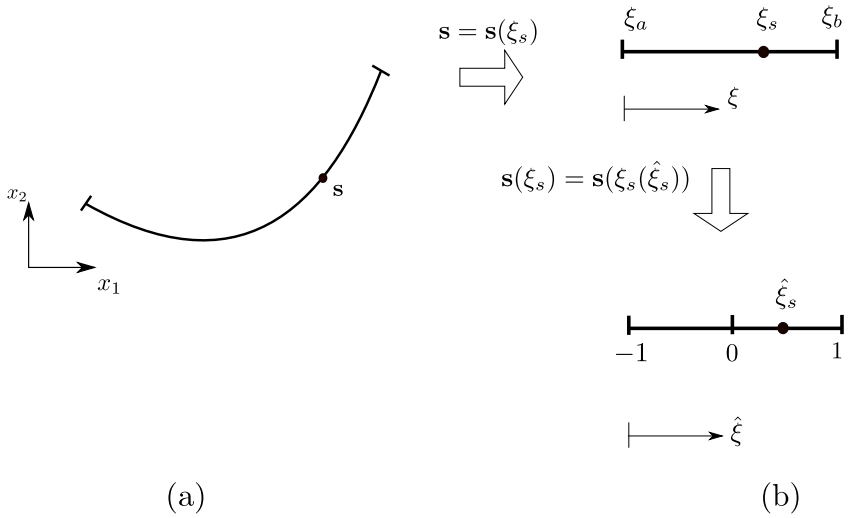

Figure 2: Coordinate system in IGABEM: (a) the element containing collocation point $\mathbf{s}$ in the global space; (b)the parametric space and parent space

strongly-singular equation can be transformed into the regularized form:

$$\int_\Gamma T_{ij}(\mathbf{s},\mathbf{x})(u_j(\mathbf{x}) - u_j(\mathbf{s}))\mathrm{d}\Gamma(\mathbf{x}) = \int_\Gamma U_{ij}(\mathbf{s},\mathbf{x})t_j(\mathbf{x})\mathrm{d}\Gamma(\mathbf{x}) \tag{24}$$

After discretisation, Equation (24) becomes

$$\sum_{e=1}^{N_e}\sum_{I=1}^{p+1} P_{ij}^I d_j^I = \sum_{e=1}^{N_e}\sum_{I=1}^{p+1} U_{ij}^I q_j^I, \tag{25}$$

where

$$P_{ij}^I = \int_{-1}^{1} T_{ij}(\mathbf{s},\mathbf{x}(\hat{\xi}))(N_I(\hat{\xi}) - N_I(\hat{\xi}_s))J(\hat{\xi})\mathrm{d}\hat{\xi} \tag{26}$$

A major advantage of Equation (24) is the fact, that it allows weaker continuity of NURBS functions at the collocation points, in comparison with Equation (6), and does not require calculation of jump term $c_{ij}(\mathbf{s})$. However, when Equation (24) is used at coincident points on crack surfaces, only singularity corresponding to one of the points is removed. There have been many attempts to overcome this difficulty. Such as, for example, creating artificial integration surfaces, which exclude the second singular point [59][60]. However, the creation and evaluation for the artificial surface is not very efficient [61] and particularly, it is cumbersome to deal with in the framework of isogeometric analysis. Therefore, in present work, Equation (24) is used only on non-cracked boundary, while on crack surfaces, the approach, known as the singularity subtraction technique (SST), is used [62]. SST is applied to both, strongly-singular and hyper-

singular integrals after the parametrization in the parent space Equations (20), (22) and (23). The essential idea of the method is to expand the kernel, the shape function and the Jacobian $J(\hat{\xi})$ into Taylor series in the vicinity of the collocation point, and split the integrands into regular and singular parts. Then the singular terms can be evaluated analytically, while for regular terms standard Gauss quadrature is used. Take the hyper-singular integral term S^e_{ijl} as example:

$$S^I_{ij} = \int_{-1}^{1} S_{ij}(\mathbf{s}, \mathbf{x}(\hat{\xi}))N_I(\hat{\xi})J(\hat{\xi})\mathrm{d}\hat{\xi} = \int_{-1}^{1} F(\hat{\xi_s}, \hat{\xi})\mathrm{d}\hat{\xi}, \tag{27}$$

The function $F(\hat{\xi_s}, \hat{\xi})$ can be expanded as:

$$F(\hat{\xi_s}, \hat{\xi}) = \frac{F_{-2}(\hat{\xi_s})}{\delta^2} + \frac{F_{-1}(\hat{\xi_s})}{\delta} + O(1) \tag{28}$$

where $\delta = \hat{\xi} - \hat{\xi_s}$. The details to obtain F_{-2} and F_{-1} with NURBS basis are given in Appendix A and can be referred in [62][27]. The final form of (27) is given by:

$$\begin{aligned}\int_{-1}^{1} F(\hat{\xi_s}, \hat{\xi})\mathrm{d}\hat{\xi} = \int_{-1}^{1} \left(F(\hat{\xi_s}, \hat{\xi}) - \frac{F_{-2}(\hat{\xi_s})}{\delta^2} - \frac{F_{-1}(\hat{\xi_s})}{\delta} \right) \mathrm{d}\hat{\xi} \\ + F_{-2}(\hat{\xi_s}) \left(-\frac{1}{1-\hat{\xi_s}} + \frac{1}{-1-\hat{\xi_s}} \right) \\ + F_{-1}(\hat{\xi_s}) \ln \left| \frac{1-\hat{\xi_s}}{-1-\hat{\xi_s}} \right|\end{aligned} \tag{29}$$

In the Equation (29) it is implied that $-1 < \hat{\xi_s} < 1$, i.e. the collocation point is located inside the element of integration. The first integral in (29) is regular and it is evaluated using standard Gaussian quadrature.

3.4 Partition of unity enrichment formulation

The partition of unity (PU) enrichment method has been well applied in FEM to model the problems with *a priori* knowledge about the solution. The approximation of the primary field by PU enrichment is decomposed by two parts: an regular part and enriched part. The later one allows the approximation to carry the specific information of the solution through additional degrees of freedom. Simpson *et al* [27] first proposed the idea of enrichment in BEM to capture the stress singularity around the crack tip. The enriched displacement approximation with

NURBS basis is:

$$u_i(\mathbf{x}) = \sum_{I \in \mathcal{N}_I} N_I(\mathbf{x}) d_i^I + \sum_{J \in \mathcal{N}_J} N_J(\mathbf{x}) \sum_{l=1}^{4} \phi_l(\mathbf{x}) a_i^J, \tag{30}$$

where d_i^I are the regular DOFs. a_i^J are the crack tip enriched DOFs. Since in BEM the crack has been explicitly modeled by two overlapped surfaces, the Heaviside enrichment is excluded. $\mathcal{N}_I$ and $\mathcal{N}_J$ are the collections of regular control points and enriched control points, respectively. The crack tip enrichment functions are defined as:

$$\{\phi_l(r,\theta), l = 1,4\} = \left\{ \sqrt{r}\sin\frac{\theta}{2}, \sqrt{r}\cos\frac{\theta}{2}, \sqrt{r}\sin\frac{\theta}{2}\sin\theta, \sqrt{r}\cos\frac{\theta}{2}\sin\theta \right\}, \tag{31}$$

where (r,θ) is the polar coordinate system associated with the crack tip. If the enrichment is done in a small vicinity of the crack tip, where the crack can be regarded as a straight line, i.e. in Equation (31) angle $\theta = \pm\pi$ and the set of four crack tip enrichment functions can be reduced to one, i.e. $\phi = \sqrt{r}$. Then Equation (32) results in:

$$u_i(\mathbf{x}) = \sum_{I \in \mathcal{N}_I} N_I(\mathbf{x}) d_i^I + \sum_{J \in \mathcal{N}_J} N_J(\mathbf{x}) \phi(\mathbf{x}) a_i^J. \tag{32}$$

Substituting the above equation into (6) and (9) and discretising with NURBS basis, the enriched displacement and traction boundary integral equations can be obtained, respectively:

$$\sum_{I}^{p+1} C_{ij}^I(\mathbf{s})(d_j^I + \phi(\mathbf{s}) a_j^I) + \sum_{e=1}^{N_e} \sum_{I}^{p+1} (T_{ij}^I d_j^I + T_{ij}^I \phi a_j^I) = \sum_{e=1}^{N_e} \sum_{I}^{p+1} U_{ij}^I q_j^I \tag{33}$$

$$\sum_{I}^{p+1} C_{ij}^I(\mathbf{s}) t_j^I + \sum_{e=1}^{N_e} \sum_{I}^{p+1} (S_{ij}^I d_j^I + S_{ij}^I \phi a_j^I) = \sum_{e=1}^{N_e} \sum_{I}^{p+1} K_{ij}^I q_j^I \tag{34}$$

Note that topological enrichment is used, i.e., only the element at the crack tip is enriched, the enrichment terms do not need to be computed for unenriched element. Differing from [27] where the discontinuous quadratic Lagrange element are enriched, the enrichment for NURBS basis will lead to blending elements due to the continuity of the basis. The singular integration for enriched element can be done with SST as before as long as the local expansion for $\phi = \sqrt{r}$ is obtained.

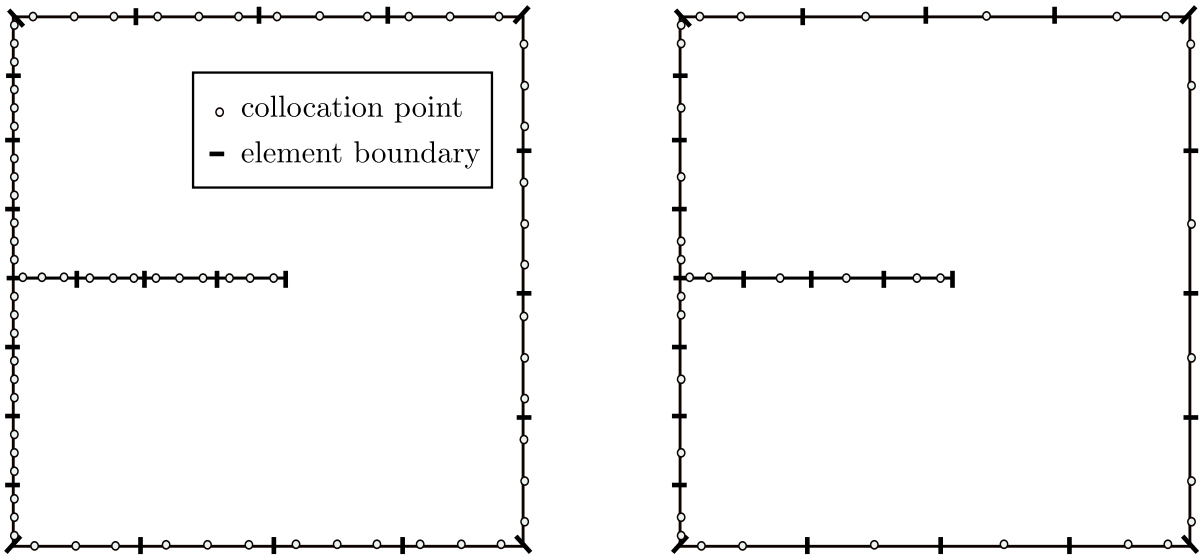

(a) (b)

Figure 3: Mesh discretization for mode I crack: (a) discontinuous Lagrange element ($p = 2$), (b) NURBS ($p = 2$)

3.5 Continuity requirements and collocation strategy

Methods of evaluating strongly-singular and hyper-singular integrals in (20), (22), (23), described above, are implicitly or explicitly based on Taylor expansion of the integrands in the vicinity of the collocation point. Since the essential feature of the isogemetrical approach is to represent displacements, tractions and the geometry using the same NURBS basis functions, special attention should be paid to the continuity of NURBS basis functions at the collocation points.

In the classical boundary element method the common way to guarantee the existence of integrals in (20), (22), (23) is by use of so-called discontinuous quadratic Largange elements [4], i.e. placing collocation points inside an element, where the quadratic polynomials are C^{∞} continuous. The same approach can be implemented with NURBS parametrisation, since inside the elements NURBS basis functions are infinitely smooth, i.e. the SST can be used directly to treat all singularities. In Figure 3 (a) and (b) the examples of boundary discretization are shown for classical and IGABEM respectively, where the collocation points in IGA are generated by Greville abscissae [63] and the collocation points are moved inside the elements when necessary.

For the enrichment formulation, Since enriched DOFs are introduced, additional source points

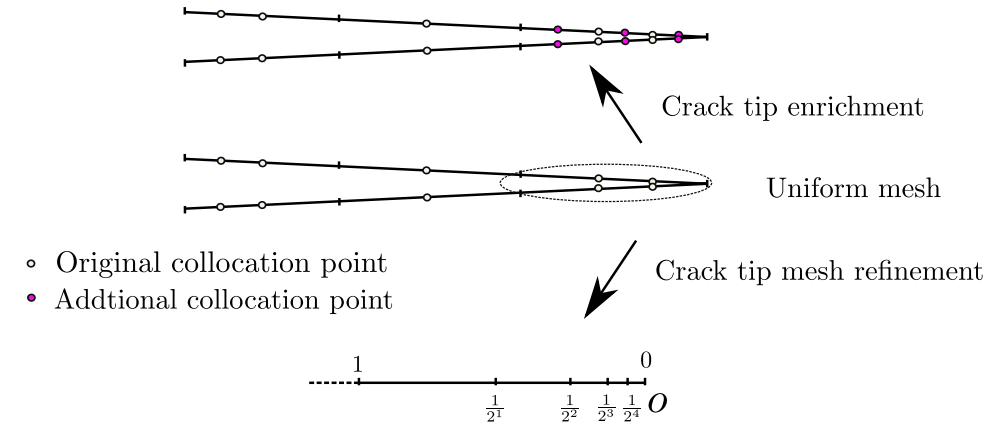

Figure 4: Mesh and collocation for crack surfaces

need to be collocated to balance the number of system unknown. The location of the source points plays an important role in the condition number of the BEM system matrix. It reveals that for crack tip enrichment, when the additional collocation points are inside the enriched element, the system condition turns out to be normal and gives accurate solution (see [27] for more details). Nevertheless, the specific location inside the crack tip element has few interference on the final results. Hence in this work, the additional source points are inserted in the crack tip element uniformly between the original collocation points. Figure (4) illustrates the scheme applied in this paper for collocation on the crack surface.

However, the classical theory of boundary integral equations admits much weaker continuity requirements, i.e. the Cauchy and Hadamard integrals exist for $C^{1,\alpha}(\Gamma)(0 < \alpha < 1)$ density functions (known as Hölder continuous) [64]. Therefore, strongly singular and hyper-singular equations, and all the more so the regularized equation (24), can be used at collocation points located at the edges of the elements in IGABEM, provided that NURBS basis is sufficiently smooth. This case corresponds to $\hat{\xi}_s = \pm 1$, therefore Equation (29) has to be modified accordingly. However, collocation strategy is a subject of further research, which requires more detailed theoretical and numerical studies.

In the present work SST is used only for the displacement BIE and traction BIE on the crack faces. On the rest of the boundary the regularized displacement BIE (24) is imposed.

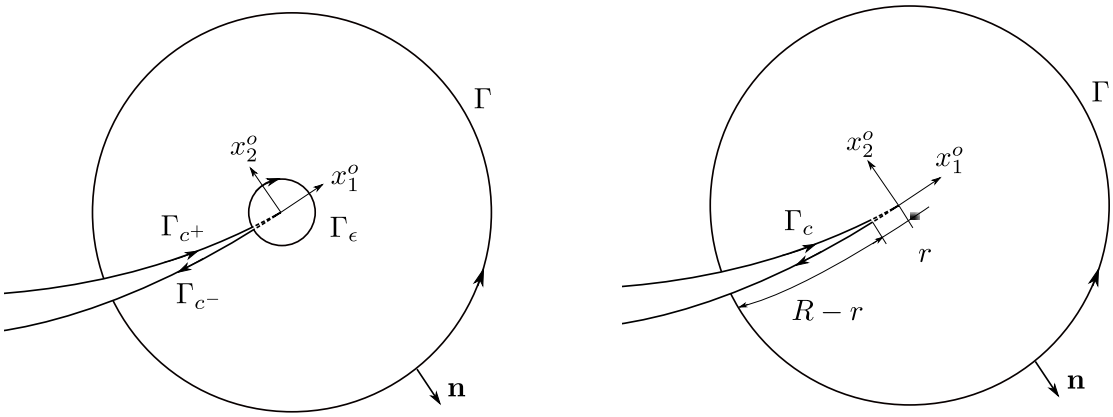

(a) (b)

Figure 5: Path definition for J integral

4 Evaluation of stress intensity factors

4.1 J_k-integral

In this section, two different kinds of J integral based methods for the extraction of SIFs are briefly reviewed. The first one is the J_k method proposed in [34], which is the more general case of the well known in fracture mechanics J integral. The definition of the J_k in 2D is given as:

$$J_k := \lim_{\Gamma_\epsilon \to 0} \int_{\Gamma_\epsilon} (W\delta_{jk} - \sigma_{ij}u_{i,k})n_j \mathrm{d}\Gamma = \lim_{\Gamma_\epsilon \to 0} \int_{\Gamma_\epsilon} P_{kj}n_j \mathrm{d}\Gamma \tag{35}$$

where P_{kj} is the Eshelby tensor, $W = 1/2\sigma_{ij}\epsilon_{ij}$ is the strain energy density, n_j is the unit outward normal of Γ_ϵ. J_1 represents a special case, known as J integral. Throughout the paper we will use these two notations interchangeably. All the variables are defined in the crack tip local coordinate system (x_0, y_0) as in Figure 5 (a). However, from the numerical point of view, it is difficult to calculate the limit in Equation (35), and the definition of J_k is usually modified in the following way. Since the integral of the Eshelby tensor is equal to zero for any closed contour, which does not contain a defect, additional countours Γ, Γ_{c^+}, Γ_{c^-} are introduced, such that Equation (35) can be rewritten as [65]

$$J_k = \lim_{\Gamma_\epsilon \to 0} \int_{\Gamma_\epsilon} P_{kj}n_j \mathrm{d}\Gamma = \int_{\Gamma} P_{kj}n_j \mathrm{d}\Gamma + \int_{\Gamma_{c^+}} P_{kj}n_j \mathrm{d}\Gamma + \int_{\Gamma_{c^-}} P_{kj}n_j \mathrm{d}\Gamma \tag{36}$$

When $k = 1$ a flat crack represents a special case, because $n_1 = 0$ along the crack surfaces, i.e.

along the contours Γ_{c^+}, Γ_{c^-}, and Equation (36) simplifies to:

$$J_1 = \int_\Gamma P_{1j} n_j \mathrm{d}\Gamma \tag{37}$$

This expression shows the path independence of J integral for flat crack. But for J_2 integral, the term from crack surface cannot be omitted since $n_2 = 1$ and this term presents singularity in numerical evaluation.

The more general scenario is seen for curved crack, the contribution from crack surfaces for both J_1 and J_2 cannot be neglected. It should be noted that the energy density $W \to 1/r$ when approaching the crack tip since both σ_{ij} and ϵ_{ij} tend to $1/\sqrt{r}$. For J_1 integral, since $n_1 \to 0$ cancels the $O(1/r)$ of the W, the integral from the crack surface can be performed as a regular one in numerical implementation. While for J_2, since n_2 tends to unity, the integral from the crack surface part will remain in $O(1/r)$ singularity, and This kind of singular integral cannot be treated in a regular way. In [65] and [34], the crack surface has been split into the far field part and near-tip part (Figure 5(b)) in order to evaluate the singular integral:

$$J_k = \int_\Gamma P_{kj} n_j \mathrm{d}\Gamma + \int_{R-r} [\![W]\!] n_k^+ \mathrm{d}\Gamma + \int_r [\![W]\!] n_k^+ \mathrm{d}\Gamma \tag{38}$$

The far field part can be integrated by regular Gauss quadrature. The near-tip part integral on the crack surface can be simply omitted for $J_1(k = 1)$, since n_1 is mostly zero, while for $J_2(k = 2)$, the near-tip part exhibits the $O(1/r)$ singularity. The energy jump $[\![W]\!]$ on the near-tip surface can evaluated as [65]:

$$[\![W]\!] = \frac{-4K_{II}\sigma_{x0}}{E\sqrt{2\pi r}} + O(r^{1/2}) \tag{39}$$

where σ_{x0} is called T-stress. Thus near-tip part of $[\![W]\!]$ can be represented as a proportion to the $r^{1/2}$

$$J_k = \int_\Gamma P_{kj} n_j \mathrm{d}\Gamma + \int_{R-r} [\![W]\!] n_k^+ \mathrm{d}\Gamma + \Lambda n_k r^{1/2} \tag{40}$$

Since two unknown variables J_2 and Λ appear in the above equation, the integral cannot be evaluated in one time. So the splitting procedure needs to be performed several times by taking different r, and a group data of J_2 and Λ can be found. Finally, least square method is used in order to find J_2 as $R = 0$. In Equation (40), as long as the $O(1/r^{1/2})$ can be captured, the

J_k integral can be correctly evaluated and the SIFs can be found consequently (see Appendix B). Nevertheless, how to choose "r" becomes path-dependent and problem-dependent in real applications.

4.2 M integral

Another way to extract the SIFs is called M integral. By applying the J integral under two states, one the real state (denoted with superscript "1"), the other the auxiliary state (superscript "2"), then adding them together, the mixed term M can be obtained:

$$J^{(1+2)} = \int_{\Gamma_\epsilon} \Big[0.5(\sigma_{ij}^{(1)} + \sigma_{ij}^{(2)})(\epsilon_{ij}^{(1)} + \epsilon_{ij}^{(2)})\delta_{1j} - (\sigma_{ij}^{(1)} + \sigma_{ij}^{(2)})\frac{\partial(u_i^{(1)} + u_i^{(2)})}{\partial x_1}\Big] n_j \mathrm{d}\Gamma \tag{41}$$

Rearranging the two state terms gives

$$J^{(1+2)} = J^{(1)} + J^{(2)} + M^{(1,2)} \tag{42}$$

where

$$M^{(1,2)} = \int_{\Gamma_\epsilon} \Big[W^{(1,2)}\delta_{1j} - \sigma_{ij}^{(1)}\frac{\partial u_i^{(2)}}{\partial x_1} - \sigma_{ij}^{(2)}\frac{\partial u_i^{(1)}}{\partial x_1}\Big] n_j \mathrm{d}\Gamma \tag{43a}$$

$$W^{(1,2)} = \sigma_{ij}^{(1)}\epsilon_{ij}^{(2)} = \sigma_{ij}^{(2)}\epsilon_{ij}^{(1)} \tag{43b}$$

Once the M integral is evaluated, the SIFs can be extracted directly (see Appendix B). But we note that in Yau *et al*'s work [33], flat crack surface is assumed. When applied to the practical problems, the radius of the contour circle should be limited to guarantee the tolerance for the assumption.

In this paper, the M integral is adopted due its efficiency. A detailed comparison for both methods applied in curved crack are investigated in the following sections.

Once the SIFs are obtained, the maximum hoop stress criterion is adopted to determine the direction of crack propagation, i.e. angle θ_c. The θ_c is found when the hoop stress reaches maximum and given as [66]:

$$\theta_c = 2\arctan\left[\frac{-2(K_{II}/K_I)}{1+\sqrt{1+8(K_{II}/K_I)^2}}\right] \tag{44}$$

5 2D NURBS crack propagation

To allow simulation of crack growth, a NURBS crack propagation algorithm is outlined next. The conceptual idea for the deformation of NURBS curve is realized by moving the control points to make the curve satisfy the external constraints under a user-defined function [67]. For crack growth problem, the external constraint is the movement of the position of crack tip (or crack front in 3D). Paluszny *et al* implemented the idea in FEM to represent crack growth or intersection by updating the control points to satisfy the constraints given by fracture parameters [68]. The algorithm is briefly reviewed as follows:

- Initiation: represent the crack by the NURBS curve.
- Define the space constraint (new position of the crack tip) M': do the BE analysis to determine the fracture parameters. then the new crack tip M' can be found by the specified fracture criterion.
- Specify the parametric constraint (parametric coordinate ξ of the old crack tip) ξ: this is the knot value of the original curve corresponding to the space constraint M'. For fracture problem, ξ denotes the old crack tip M.
- Define the localization constraint f: this is to specify the influence of the constraints. Here for 2D fracture this constraint is selected as the NURBS basis functions at parametric constraint ξ(which is called natural deformation in [67]). $f(A) = R_{A,p}(\xi)$, $A = 1, ..., n$, n is the number of NURBS basis function of the corresponding control point P_A.
- Calculating the movement vector of each control point $\mathbf{m}(A)$: the movement of the control points is given by

$$\mathbf{m}(A) = \frac{f(A)}{\sum_{B=1}^{n} R_{B,p}(\xi) f(B)} \mathbf{e}, \quad \mathbf{e} = \overrightarrow{MM'} \tag{45}$$

The process to stretch NURBS curve to simulate crack growth in 2D is illustrated in Figure 6. Certain knot insertion should be done at the crack tip element in order to capture the local changes. We note that enhancing the knot interval at the crack tip element also help to improve the solution near the crack tip, and a graded mesh refinement is designed as in Figure (4), where the new knots are inserted consecutively at the $(1/2)^i, \quad i = 1, 2, 3, 4...$ of the distance to the crack tip in the parametric space. In this work, the crack propagation angle is defined by

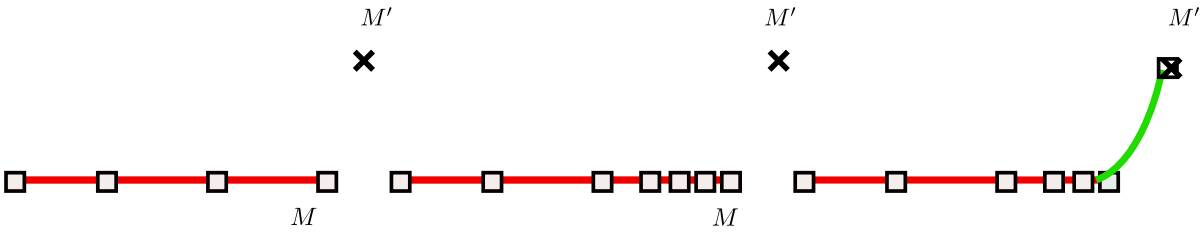

Figure 6: NURBS modification for crack growth. (a)Original crack and new crack tip M'; (b)Knot insertion to enhance the crack tip; (c)Move the control points to obtain new crack curve by the presented algorithm

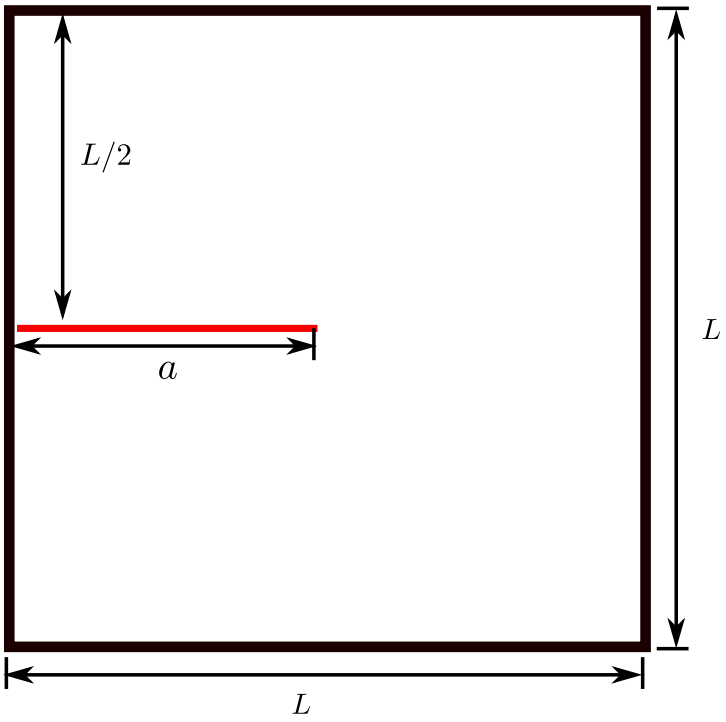

Figure 7: Edge crack

maximum hoop stress criterion and the crack advance is a user-specified constant in each step. Whereas the NURBS modification algorithm is not limited to the physical criterion as long as the constraints can be given.

6 Numerical examples

In this section, several numerical examples are presented to verify the proposed method for fracture analysis. We first give examples to study the behavior of the (X)IGABEM on static fracture analysis. Then the application for the crack propagation algorithm by comparing against an XFEM result is demonstrated.

6.1 Edge crack

Figure (7) illustrates the edge crack model with the analytical SIF-displacement solution [69] (refer to the auxiliary displacements in Appendix B) applied on the non-crack boundary and zero traction is specified to the crack. The parameters $E = 1$, $\nu = 0.3$, $a = 1$, $L = 2$. For mode I crack, $K_I = 1, K_{II} = 0$ and for mode II, $K_I = 0, K_{II} = 1$ in the displacement solution. Thus the numerical displacement on the crack as well as SIFs can be compared to the analytical solution.

In this example, we first investigate the capability of capturing the singularity at the crack tip through the enrichment, adaptive refinement and uniform mesh through mode I crack. Then the SIFs comparison is made under uniform meshes between Lagrange element and NURBS element.

6.1.1 Studying on capturing crack tip singularity

Accurate approximation of the solutions near the crack tip is crucial to a more accurate evaluation of fracture parameters like SIFs. Three scenarios are studied here, the uniform mesh, the graded refinement of crack tip element and the enrichment of crack tip element. The latter two is based on the uniform mesh. Figure (8) shows the displacement u_y along upper crack surface for mode I problem. The crack is discretised by 3 uniform elements. It can be observed that the all the numerical displacements agrees well with analytical solution, although the mesh is coarse, and the graded refinement and enrichment method gives a better result near the crack tip. To further assess the accuracy of these methods, the error of displacement L_2 norm on the crack surfaces which is given as

$$e_{L_2} = \sqrt{\frac{\int_{\Gamma_c} (\mathbf{u} - \mathbf{u}_{ext})^{\mathrm{T}} (\mathbf{u} - \mathbf{u}_{ext}) \mathrm{d}\Gamma}{\int_{\Gamma_c} \mathbf{u}_{ext}^{\mathrm{T}} \mathbf{u}_{ext} \mathrm{d}\Gamma}} \tag{46}$$

is plotted in Figure (9). It should be noted that the graded refinement for crack tip element by knot insertion described in Figure (4) cannot be done with infinite times in practice. With more knots inserted, higher and higher accuracy can be obtained, however, the system condition becomes worse due to the concentration of collocation points near the crack tip. So we only checks the convergence results by inserting the knots at $(1/2)^i$ consecutively until $i = 4$. It

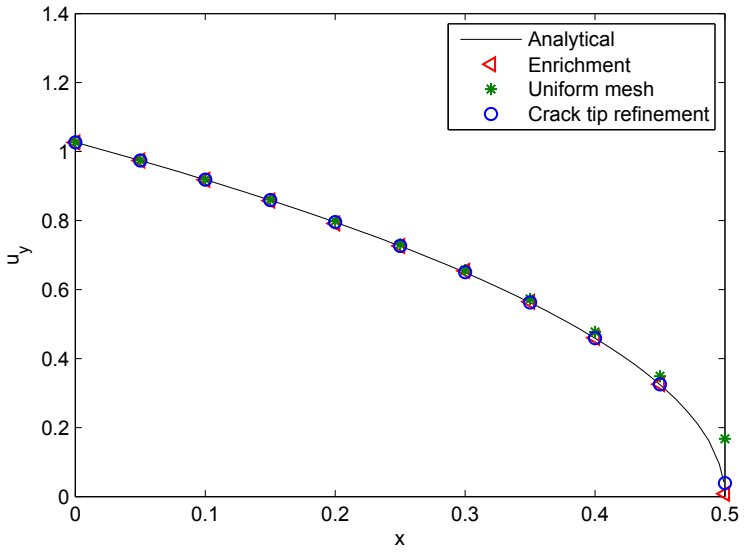

Figure 8: u_y along the upper crack surface

can be seen that enrichment achieves an accuracy between those by the knot insertion of 3 and 4 times for the crack tip element while the convergence rate is improved. In the following examples for static crack and crack propagation, only the graded mesh refinement by 4 times knot insertion is studied further.

6.1.2 SIFs comparison with Lagrange basis

To give a basic cognition for the IGABEM for fracture, the SIFs given by M integral are compared to that from Lagrange element under uniform mesh without any special treatment for crack tip. A convergence check for the error of normalized SIFs K_I, K_{II} is shown in Figure (10). It can be observed that the precision with NURBS is much better than that of discontinuous Lagrange basis. It may not be fair to compare them as in Figure (3) since discontinuous Lagrange basis introduces too many nodes in average. Thus the convergence results is re-plotted in terms of element number per edge in Figure (11). In the initial mesh models, the result of K_I from Lagrange basis is better than NURBS, but with the mesh further refined, the results from NURBS tend to be more accurate results.

Further investigation on SIFs evaluation by graded mesh refinement is done in the following examples.

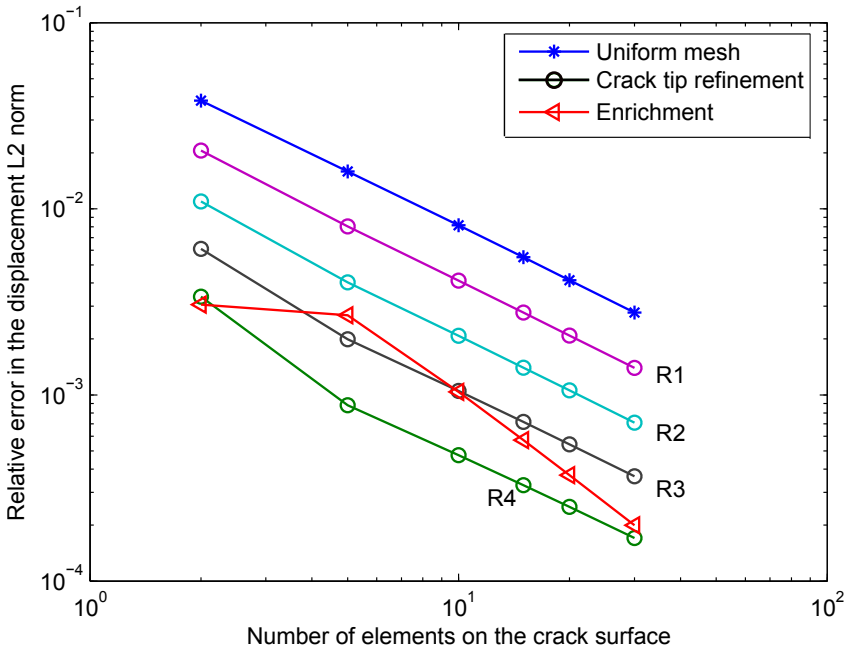

Figure 9: Relative error in L_2 norm of the displacement along the crack surface. Note that $R1$, $R2$, $R3$ and $R4$ represents the crack tip element is refined by knot insertion at $(1/2)^1$, $(1/2)^2$, $(1/2)^3$ and $(1/2)^4$, respectively

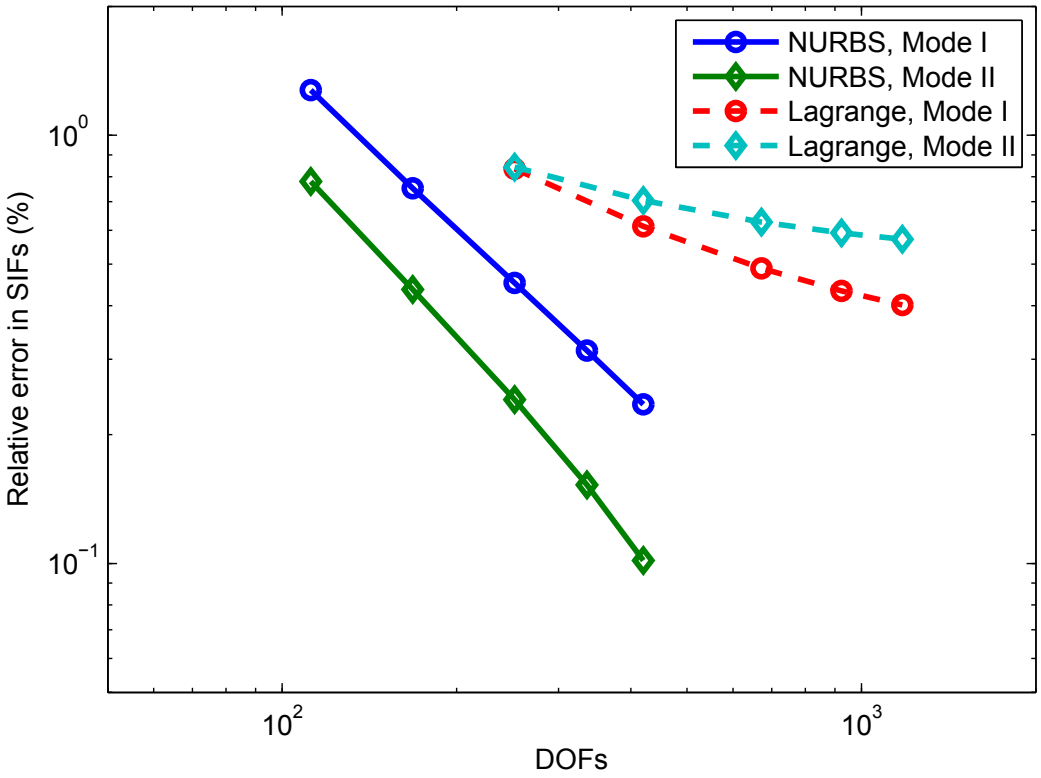

Figure 10: Convergence results of SIF for mode I and II crack

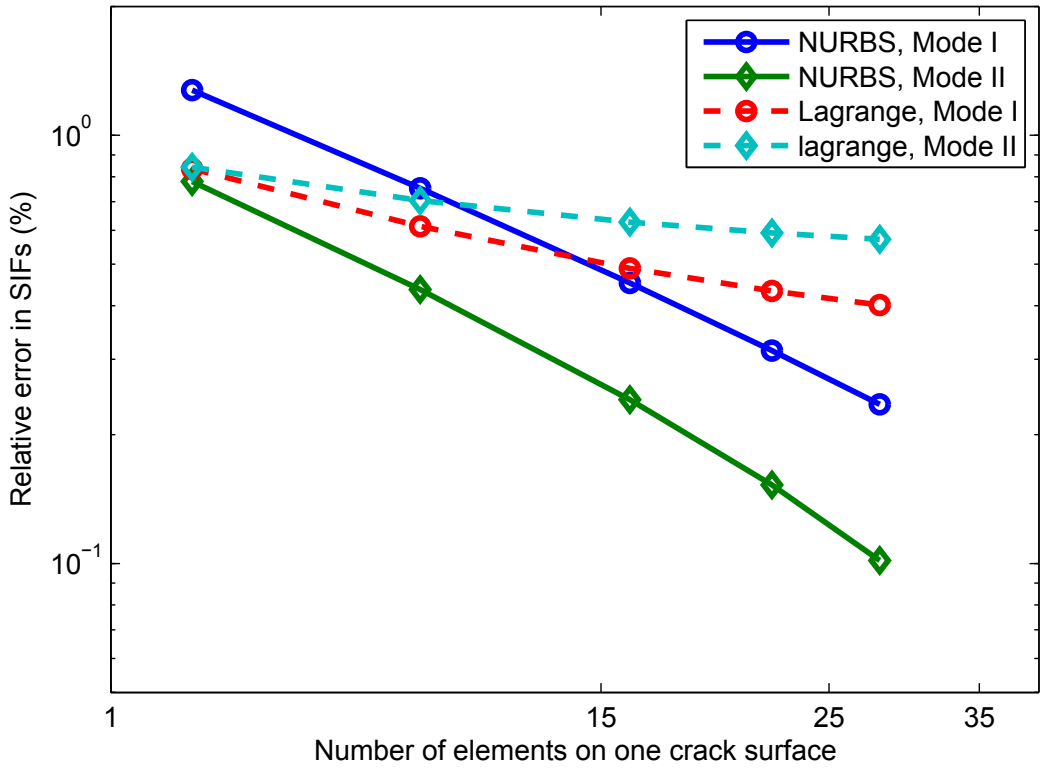

Figure 11: Convergence results of SIF for mode I and II crack, plotting in terms of element number

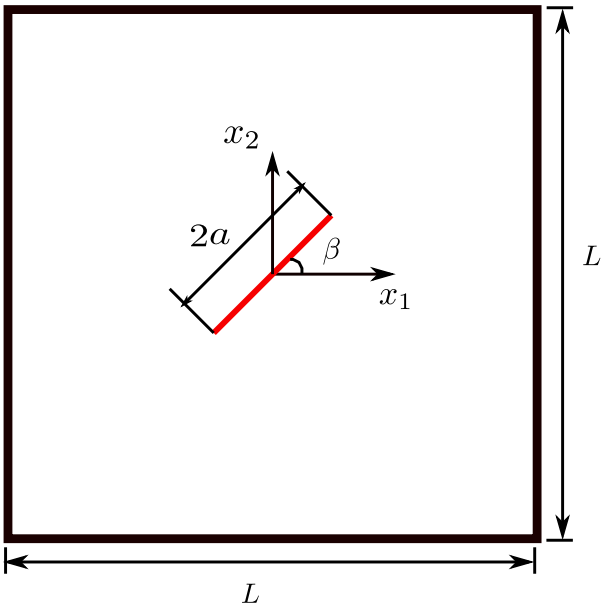

Figure 12: Physical model of inclined center crack problem

6.2 Inclined centre crack

In this example, The SIFs are further calculated for a plate with an inclined crack under remote biaxial tension such that $\sigma = \sigma_0$ is applied in y-direction and $\sigma = \lambda\sigma_0$ is applied in x-direction, where λ is the load ratio and $\sigma_0 = 1$. The inclined centre crack with the angle β varies from 0 to $\pi/2$, see Figure (12). The edge length of the plate $L = 1$, crack length $2a = 0.02$. $L >> a$ so that the numerical results can be compared with the analytical solution for an infinite plate, given in [70]. The material parameters $E = 1$, $\nu = 0.3$. The SIFs in this example obtained by M integral can be compared to the analytical ones as follows:

$$K_I = \sigma\sqrt{\pi a}(\cos^2\beta + \lambda\sin^2\beta) \tag{47a}$$

$$K_{II} = \sigma\sqrt{\pi a}(1-\lambda)\cos\beta\sin\beta \tag{47b}$$

Here 2 uniform elements are used on non-crack geometry. The mesh of the crack surface has been refined uniformly for both discontinuous Lagrange basis BEM (LBEM) and NURBS (IGABEM). The local graded refinement for crack tip element described in Figure (4) is also performed based on the uniform refinement (the corresponding result is denoted as IGABEM(r)). Assuming the number of elements for crack is m, a convergence check is done with crack angle $\beta = \pi/6$ at the load ratio $\lambda = 0.5$ (biaxially loaded). The results are given in Table (1) and (2). Here the

SGBEM results [13] are also given as a reference. It can be concluded that the proposed local crack tip refinement gives a very good accuracy for practical applications.

Then SIFs are compared for different angles at $\lambda = 0$ (uniaxially loaded). In this case, the crack is discretized by 4 uniform elements, and for IGABEM, the crack tip element is further refined in the same fashion. The SIFs are given in Table (3).

	K_I/K_I^{exact}			
m	SGBEM	LBEM	IGABEM	IGABEM(r)
3	0.9913	1.00451	1.00982	1.00120
4	1.0002	1.00333	1.00769	1.00105
5	1.0001	1.00268	1.00633	1.00090
6	1.0002	1.00230	1.00539	1.00080
7	1.0003	1.00206	1.00474	1.00074
8	1.0003	1.00190	1.00426	1.00070
9	1.0003	1.00177	1.00389	1.00066
10	1.0003	1.00167	1.00359	1.00064
11	1.0003	1.00159	1.00336	1.00062
12	1.0003	1.00152	1.00316	1.00060
14	1.0003	1.00142	1.00285	1.00058

Table 1: Normalized K_I in inclined centre crack

	K_{II}/K_{II}^{exact}			
m	SGBEM	LBEM	IGABEM	IGABEM(r)
3	1.0075	1.00104	1.00647	1.00146
4	1.0009	1.00129	1.00656	1.00129
5	1.0010	1.00158	1.00607	1.00113
6	1.0009	1.00160	1.00550	1.00102
7	1.0014	1.00153	1.00500	1.00096
8	1.0005	1.00143	1.00458	1.00091
9	0.9997	1.00134	1.00424	1.00087
10	1.0009	1.00126	1.00396	1.00085
11	0.9992	1.00119	1.00373	1.00083
12	1.0013	1.00112	1.00353	1.00081
14	1.0004	1.00102	1.00322	1.00079

Table 2: Normalized K_{II} in inclined centre crack

6.3 Arc crack

The circular arc crack under remote uniform biaxial tension is checked to further validate the effectiveness of the proposed method. The problem is defined in Figure (13). Here $L = 1$, $2a = 0.01$, $L >> a$, $E = 1$, $\nu = 0.3$. In the test $\sigma = 1, \beta = \pi/4$. The analytical SIFs are given

	K_I			K_{II}		
β	Exact	IGABEM(r)	SGBEM	Exact	IGABEM(r)	SGBEM
0	1.0000	$1.0006(6.0e-4)$	$1.0002(2.0e-4)$	0.0000	$0.0000(<1.e-4)$	$0.0000(<1.e-4)$
$\pi/12$	0.9330	$0.9336(6.4e-4)$	$0.9332(2.1e-4)$	0.2500	$0.2503(1.2e-3)$	$0.2502(8.0e-4)$
$\pi/6$	0.7500	$0.7505(6.7e-4)$	$0.7502(2.7e-4)$	0.4330	$0.4336(1.4e-3)$	$0.4334(9.2e-4)$
$\pi/4$	0.5000	$0.5003(6.0e-4)$	$0.5001(2.0e-4)$	0.5000	$0.5006(1.2e-3)$	$0.5004(6.0e-4)$
$\pi/3$	0.2500	$0.2501(4.0e-4)$	$0.2500(<1.e-4)$	0.4330	$0.4335(1.2e-3)$	$0.4333(6.9e-4)$
$5\pi/12$	0.0670	$0.0670(<1.e-4)$	$0.0670(<1.e-4)$	0.2500	$0.2503(1.2e-3)$	$0.2502(8.0e-4)$
$\pi/2$	0.0000	$0.0000(<1.e-4)$	$0.0000(<1.e-4)$	0.0000	$0.0000(<1.e-4)$	$0.0000(<1.e-4)$

Table 3: SIFs and relative error (in the brackets) for the inclined centre crack

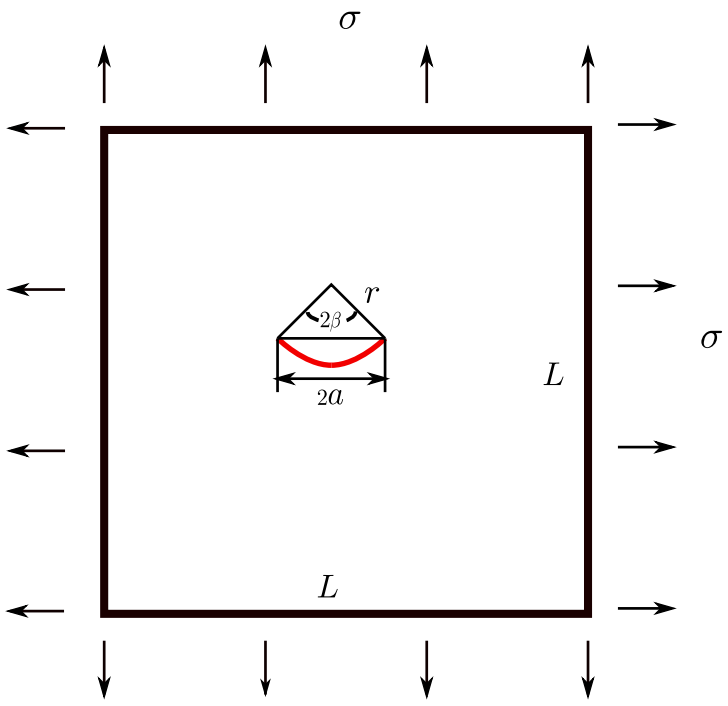

Figure 13: Physical model of arc crack

by [71] as:

$$K_I = \sigma\sqrt{\pi a}\frac{\cos(\beta/2)}{1+\sin^2(\beta/2)} \tag{48a}$$

$$K_{II} = \sigma\sqrt{\pi a}\frac{\sin(\beta/2)}{1+\sin^2(\beta/2)} \tag{48b}$$

2 elements are used for non-crack edge and m elements are used to discretize the cracks with crack tip elements refined as in Figure (4). A convergence check for SIFs are listed in Table 4. Here the SIF extraction from both J_k integral method and M integral method is compared for contour integration. Both methods use a same radius R, and the partition of the crack surface for J_k integral is done by experience at $r = 0.03R, 0.04R, 0.05R, 0.06R, 0.07R$. It can be found that the results of the two methods are comparable. But we note that the J_k integral method is more computationally expensive than M integral as 1)it needs to integrate on crack surface; 2) the crack surface needs to be partitioned which is not convenient in IGA; 3) the integration needs to be repeated several times in order to get a least square approximation. All these points are avoided in M integral method. What's more, the partition of the crack surface into far field and near-tip field by experience which is not robust in practical applications.

	K_I/K_I^{exact}		K_{II}/K_{II}^{exact}	
m	M integral	J_k integral	M integral	J_k integral
10	1.00045	0.99972	0.97506	1.00309
14	1.00014	0.99979	0.98621	1.00248
17	1.00011	0.99982	0.98642	1.00217
20	1.00009	0.99985	0.98657	1.00195
23	1.00002	0.99987	0.99407	1.00176
26	1.00002	0.99989	0.99413	1.00163

Table 4: SIFs in arc crack

6.4 Crack growth in plate with rivet holes

Crack propagation by IGABEM is checked in this case. The problem is adopted from the XFEM work by Moës *et al* [25]. The geometry and load condition are illustrated in Figure 14. The material parameters $E = 1000$, $\nu = 0.3$. 12 elements are used for each circle and 3 elements for each edge and initial cracks. The crack tip elements are further refined (without enrichment) by the way described in previous section so that the knot level is enhanced for stretching the crack. The same parameters ($\theta = \pi/4$, initial crack length $a = 0.1$) are used in order to compare the crack evolution path directly.

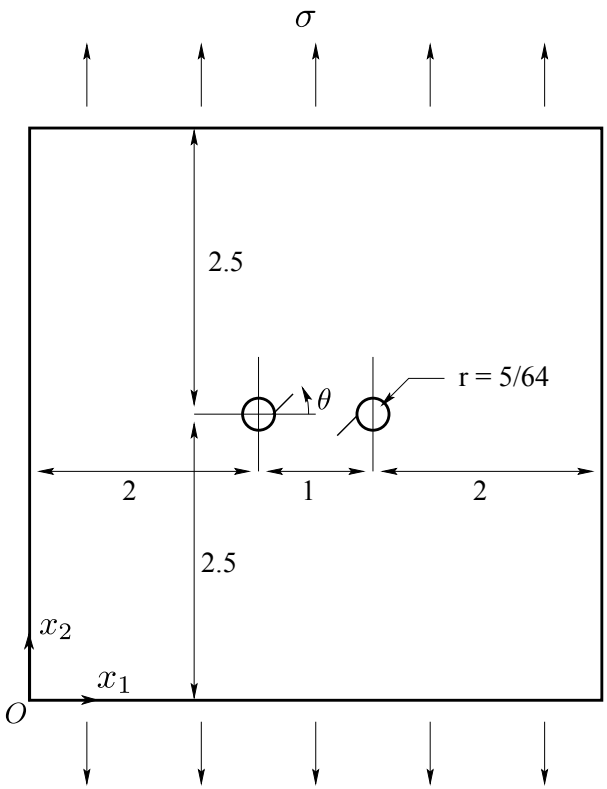

Figure 14: Physical model of rivet holes plate with initial cracks emanated from holes. The initial crack lengths are 0.1, (Moës *et al*, 1999)

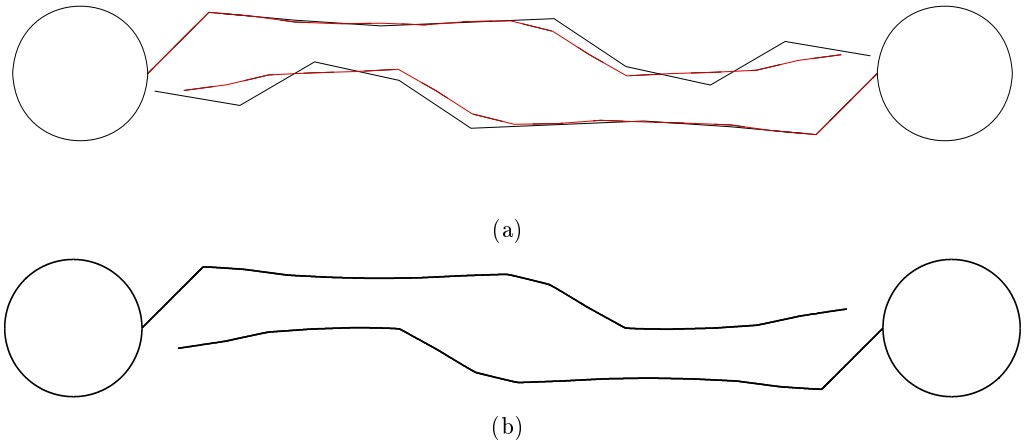

Figure 15: Crack path comparison (a)XFEM (Moës *et al*, 1999), $\Delta a = 0.1$ for black lines and $\Delta a = 0.05$ for red lines; (b)IGABEM, $\Delta a = 0.05$ for black lines

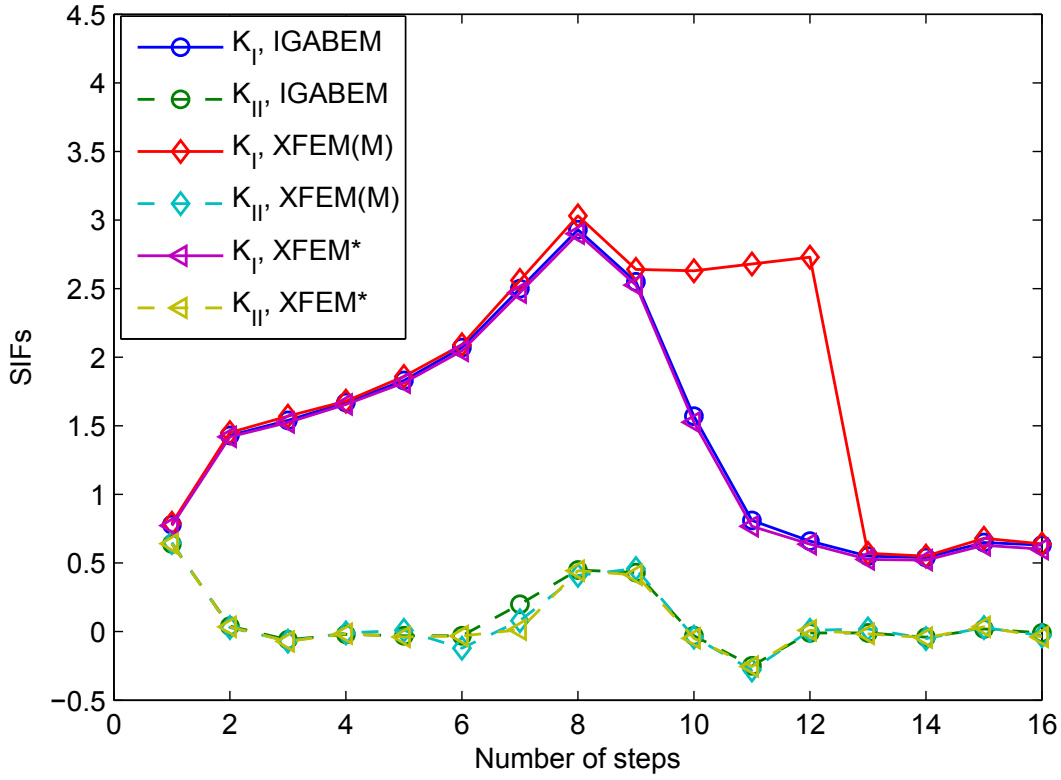

Figure 16: SIF comparison for the whole process of crack propagation. XFEM(M) is from Moës *et al*, 1999, XFEM* is from the in-house XFEM code

Assume that crack advance Δa in each step is a constant and $\Delta a = 0.05$, which is the same as the fine mesh model in [25]. the crack has propagated 16 steps and the crack path obtained by IGABEM is shown in Figure (15). It fits well compared to the red path by XFEM and the IGABEM path seems a bit smoother than the XFEM result. The tip position and SIFs in each step are further compared(Table (5)). It can be observed that the tip position is generally equivalent. However, the SIFs show significant difference for some steps, as plotted in Figure (16).

6.5 Three holes plate bending problem

The example of three point bending beam with three holes is simulated to further check the robustness of IGABEM for crack propagation. The geometry and load condition are illustrated in Figure (17). The material parameters $E = 1000$, $\nu = 0.37$ are used in the simulations. Plane strain condition is assumed. With the variation of the position of the initial crack, different crack trajectories are obtained by experiment [72]. Here the position of the initial crack is set as

	IGABEM		XFEM*		XFEM(M)	
Step	x_c	y_c	x_c	y_c	x_c	y_c
Initial	2.1488	2.5707	2.1488	2.5707	2.1488	2.5707
1	2.1986	2.5665	2.1986	2.5662	2.1986	2.5663
2	2.2481	2.5596	2.2481	2.5593	2.2481	2.5595
3	2.2981	2.5575	2.2981	2.5570	2.2981	2.5575
4	2.3481	2.5564	2.3480	2.5556	2.3481	2.5581
5	2.3981	2.5573	2.3980	2.5564	2.3981	2.5562
6	2.4480	2.5598	2.4480	2.5587	2.4480	2.5600
7	2.4980	2.5614	2.4979	2.5604	2.4980	2.5608
8	2.5463	2.5485	2.5463	2.5477	2.5465	2.5488
9	2.5885	2.5217	2.5885	2.5209	2.5886	2.5219
10	2.6324	2.4978	2.6324	2.4968	2.6321	2.4972
11	2.6824	2.4986	2.6823	2.4990	2.6820	2.4998
12	2.7324	2.5000	2.7323	2.4997	2.7320	2.5013
13	2.7823	2.5035	2.7821	2.5036	2.7819	2.5037
14	2.8311	2.5144	2.8307	2.5157	2.8306	2.5151
15	2.8805	2.5217	2.8802	2.5223	2.8802	2.5217

Table 5: Tip position for left crack tip with $\Delta a = 0.05$ in. XFEM(M) is from Moës *et al*, 1999, XFEM* is from the in-house XFEM code

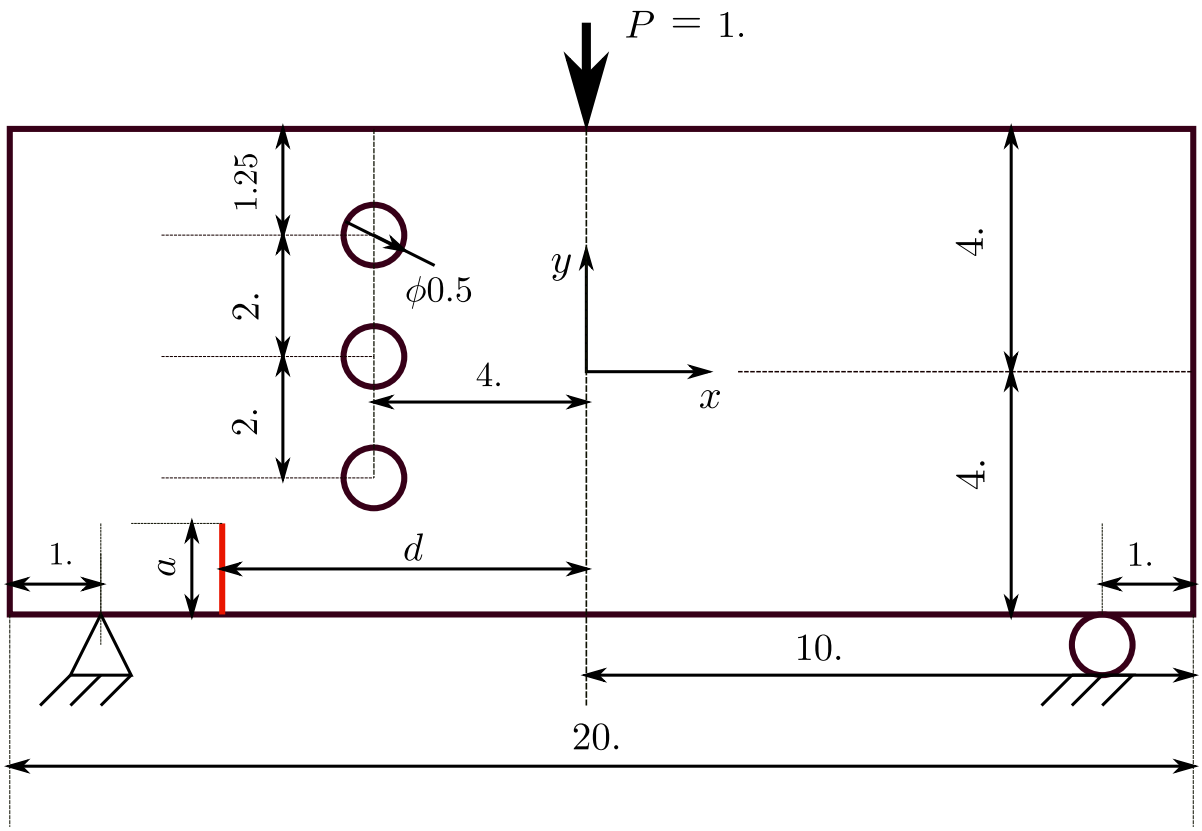

Figure 17: Physical model of three points bending beam with 3 holes

$d = 5$ in, $a = 1.5$. This example has been reported by using XFEM and XEFG [73] as well. The crack advance Δa is set to be 0.052 in for both XFEM and IGABEM. The model is discretized by 27869 nodes and 55604 triangular elements for XFEM. And for IGABEM, 82 elements and 230 DOFs are used. Crack tip mesh refinement is used without enrichment. It is not mentioned in [73] about the XEFG model size, and the crack increment $\Delta a = 0.1$ for XEFG. Figure (18) and Figure (19) compares the crack growth path using all the mentioned methods. All the crack paths agree well with the experiment. Of course, due to the differences in the setup of mesh discretisation and crack increment, the numerical results are different from each other without any doubt. It can be observed from Figure 20 that the IGABEM has slightly better fitting with the crack trajectory than the XFEM when the crack pass through the first hole. Figure (21) compares the SIFs from XFEM and IGABEM. We note that significant difference occurs when crack passes nearby the first hole. A possible explanation for this could be that in XFEM the size of the pr-enriched zone is too big and interferes with the outer boundary, where the asymptotics of the solutions is different from $\sqrt{r}$ while in IGABEM, since adaptive mesh refinement is performed, no any priori assumption is made.

6.6 Crack propagation in an open spanner

The last example is to simulate the failure process of an open spanner due to the crack propagation, in which the geometry is taken directly from CAD. The physical configuration is shown in Figure (22). Assuming that a small defect has initiated from the surface at the area of the high concentrated stress from elastostatic analysis [47]. The initial geometry with the crack for analysis is given in Figure (23). The crack will grow at $\Delta a = 0.1$. Figure (24) presents the deformed geometry with crack. This example gives a straightforward illustration the concept of the seamless incorporation of CAD and failure analysis.

7 Conclusion

A detailed procedure to model linear elastic fracture problem using the NURBS based IGABEM is proposed in this work. The dual BIEs is introduced so that cracks can be modeled in a single domain. Different treatments for crack tip singularity are investigated including crack tip graded mesh refinement and partition of unity enrichment. The popular approaches to extract SIFs

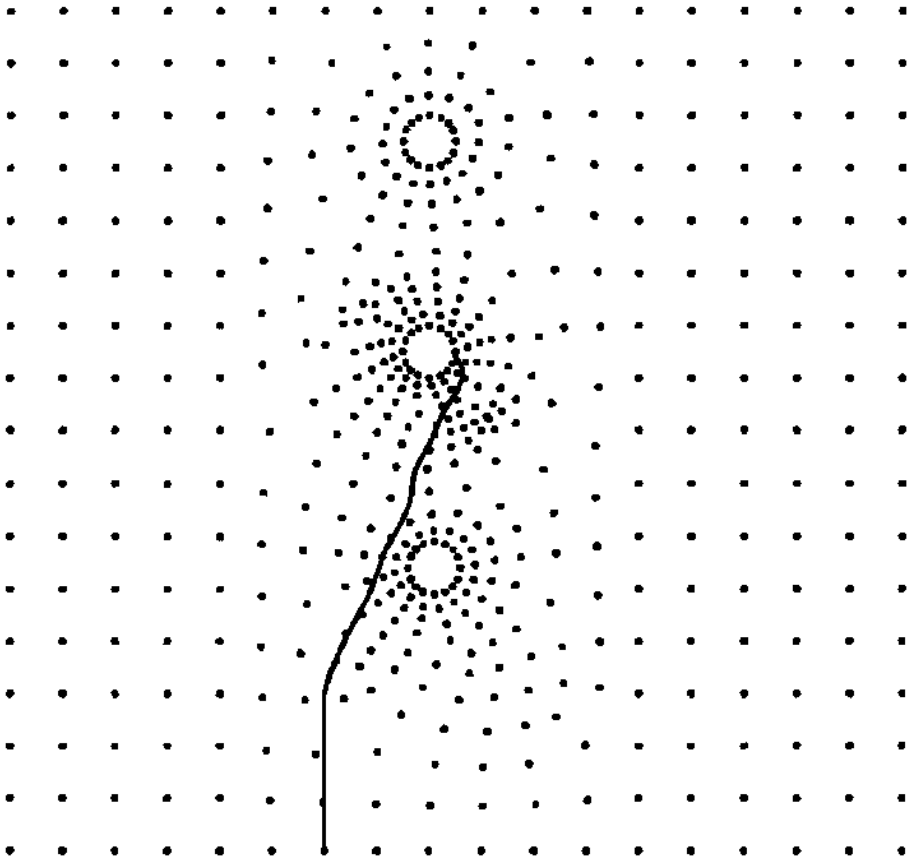

Figure 18: Crack path by XEFG at $\Delta a = 0.1$ (Ventura *et al*, 2002)

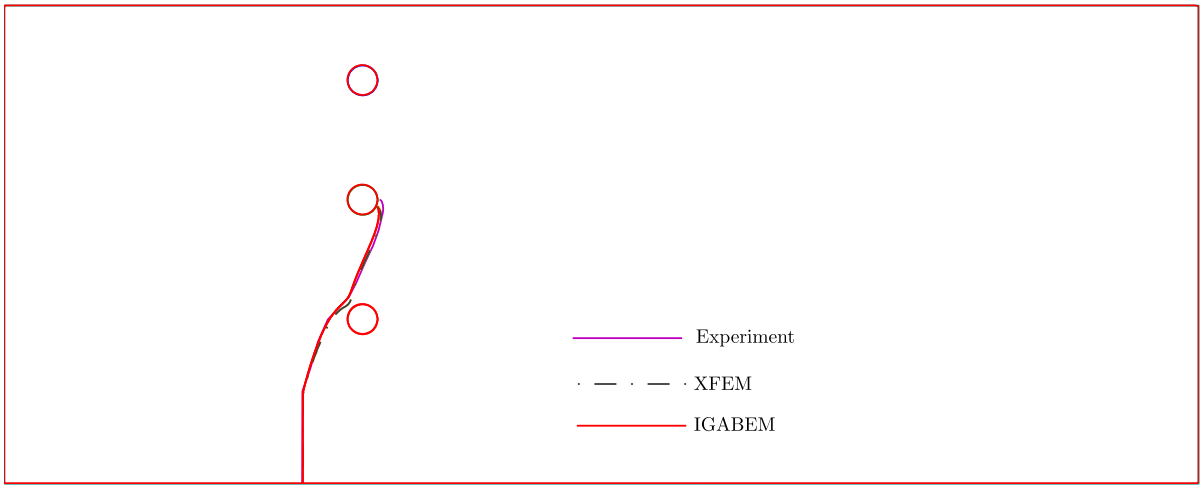

Figure 19: crack path

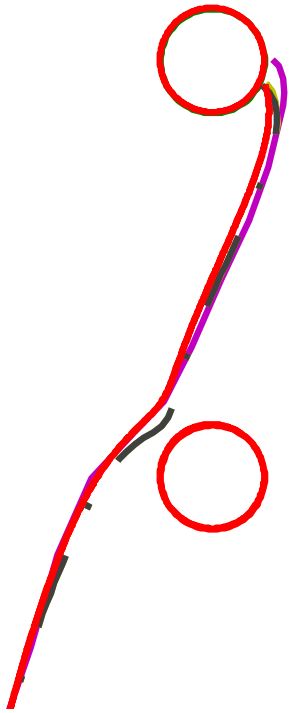

Figure 20: Zoom plot of the crack path

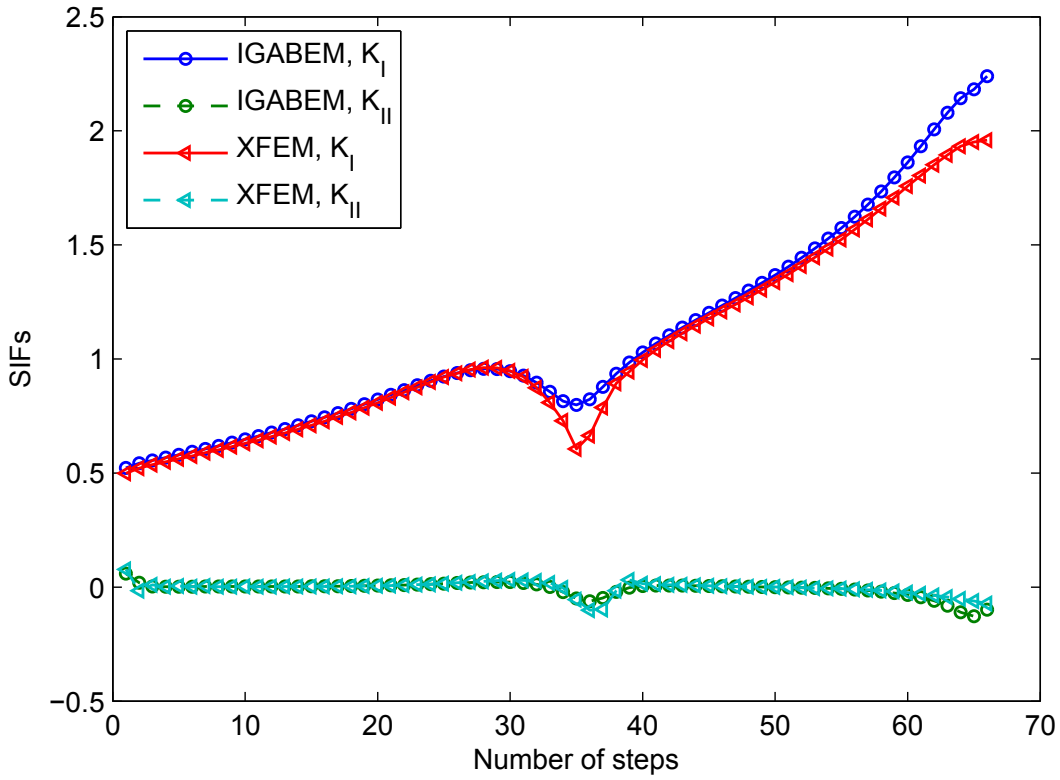

Figure 21: Comparison of the SIFs for the whole process of crack propagation

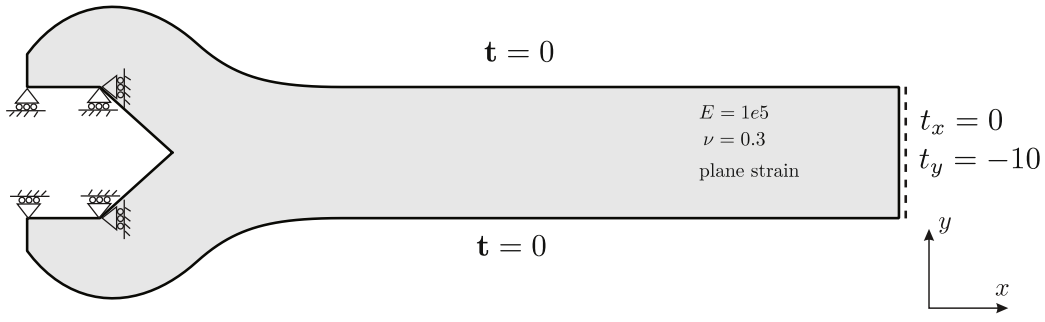

Figure 22: Boundary conditions, materials and geometry of the open spanner (Simpson *et al*, 2012)

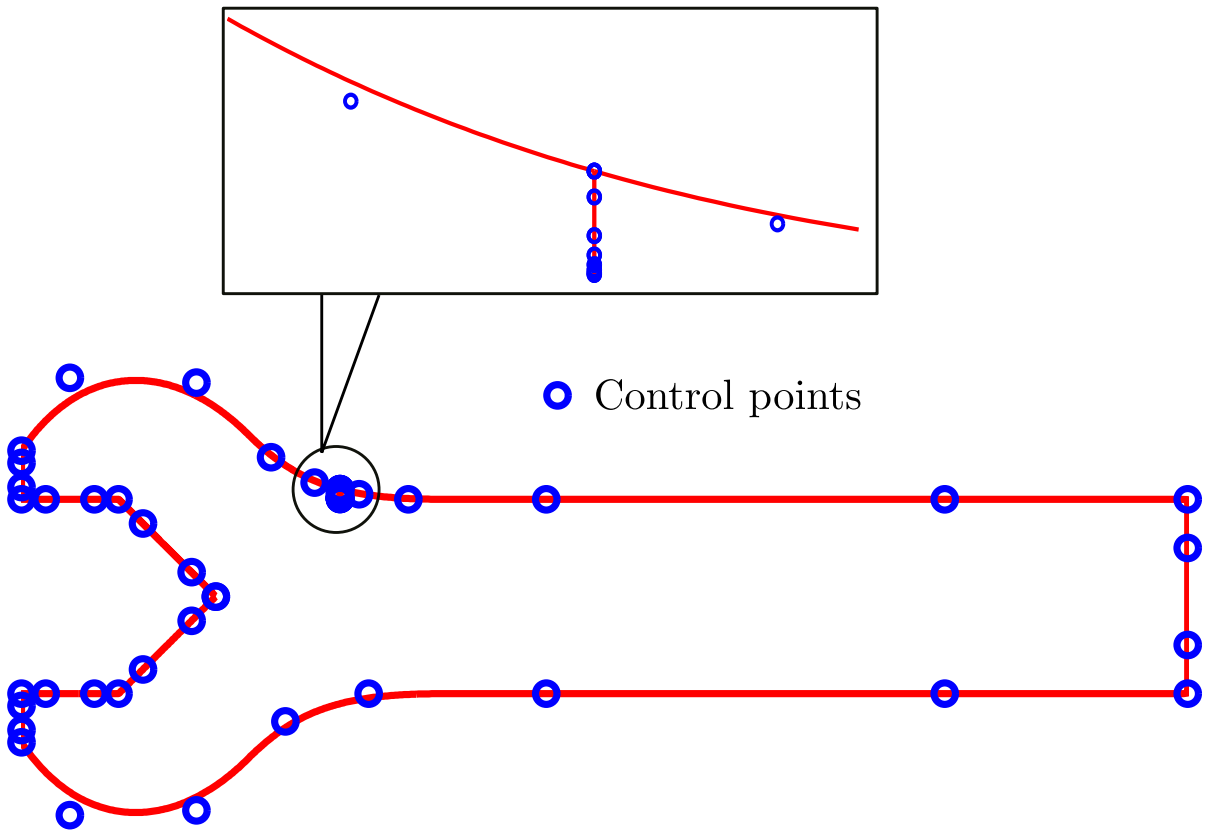

Figure 23: Control points and NURBS curve of the open spanner

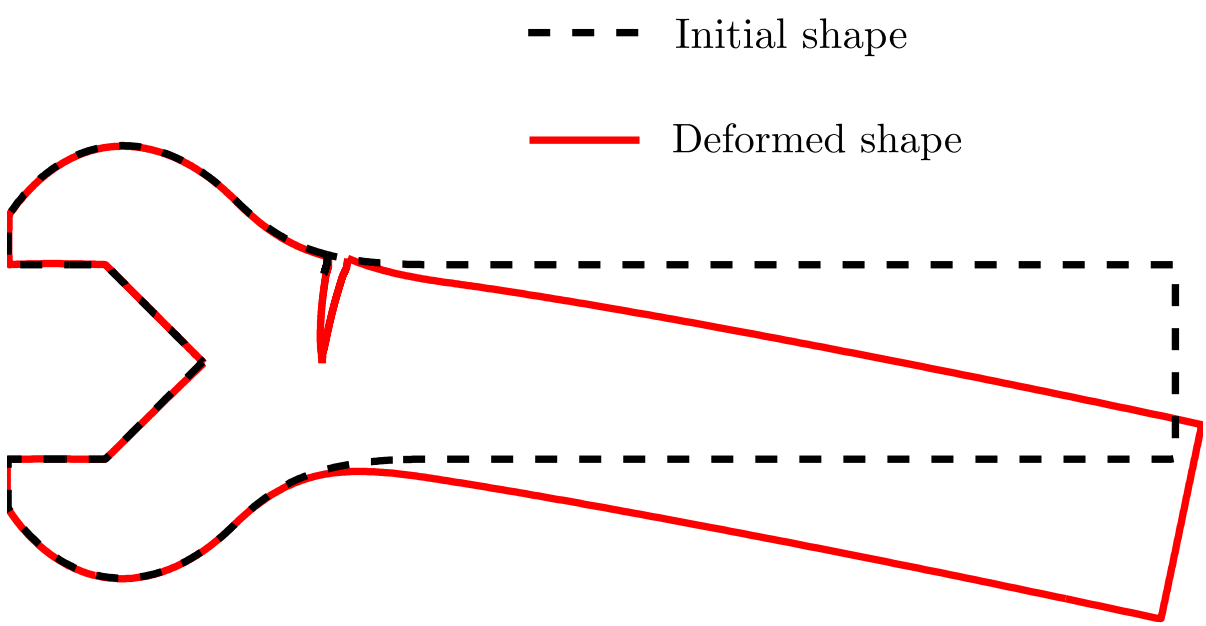

Figure 24: The deformed geometry after 10 steps crack propagation

are compared in the framework of IGABEM and it proves that the M integral is more efficient for SIF extraction in IGABEM. The cracks are modeled directly by NURBS, and an algorithm for modifying the NURBS curve is implemented to describe the crack propagation. Numerical examples shows that:

(1) The IGABEM can obtain a higher accuracy than Lagrange basis based BEM for the same model size or DOFs;

(2) Both crack tip graded mesh refinement and enrichment can capture the singular behavior near the crack tip, and the graded mesh refinement is selected to apply in the crack growth;

(3) The proposed crack growth procedure can lead to C^1 smooth crack trajectory and agrees well with those results from XFEM.

The authors believe that the crack propagation in three dimensional domain would benefit more thanks to the smooth crack representation and higher order continuous NURBS basis, which would provide a distinct solution scheme for fracture analysis when compared to the idea in the framework of FEM/XFEM.

Acknowledgements

The authors would like to acknowledge the financial support of the Framework Programme 7 Initial Training Network Funding under grant number 289361 "Integrating Numerical Simulation and Geometric Design Technology".

Appendix A

The fundamental solutions for traction BIE are:

$$K_{ij} = \frac{1}{4\pi(1-\nu)r}[(1-2\nu)(\delta_{ij}r_{,k} + \delta_{jk}r_{,i} - \delta_{ik}r_{,j}) + 2r_{,i}r_{,j}r_{,k}]n_k(\mathbf{s}) \tag{49}$$

$$\begin{aligned} S_{ij} = \frac{\mu}{2\pi(1-\nu)r^2}\Big\{ & 2\frac{\partial r}{\partial n}[(1-2\nu)\delta_{ik}r_{,j} + \nu(\delta_{ij}r_{,k} + \delta_{jk}r_{,i}) - 4r_{,i}r_{,j}r_{,k}] \\ & + 2\nu(n_i r_{,j}r_{,k} + n_k r_{,i}r_{,j}) - (1-4\nu)\delta_{ik}n_j \\ & + (1-2\nu)(2n_j r_{,i}r_{,k} + \delta_{ij}n_k + \delta_{jk}n_i)\Big\}n_k(\mathbf{s}) \end{aligned} \tag{50}$$

Now we present the SST formula for the hyper-singular integral as following. Expanding the components of distance between field and source points as Taylor series in parent space gives:

$$\begin{aligned} x_i - s_i &= \frac{\mathrm{d}x_i}{\mathrm{d}\hat{\xi}}\Big|_{\hat{\xi}=\hat{\xi}_s}(\hat{\xi}-\hat{\xi}_s) + \frac{\mathrm{d}^2x_i}{\mathrm{d}\hat{\xi}^2}\Big|_{\hat{\xi}=\hat{\xi}_s}\frac{(\hat{\xi}-\hat{\xi}_s)^2}{2} + \cdots \\ &:= A_i(\hat{\xi}-\hat{\xi}_s) + B_i(\hat{\xi}-\hat{\xi}_s)^2 + \cdots \\ &= A_i\delta + B_i\delta^2 + O(\delta^3) \end{aligned} \tag{51}$$

and

$$\begin{aligned} A &:= \left(\sum_{k=1}^{2} A_k^2\right)^{\frac{1}{2}} \\ C &:= \sum_{k=1}^{2} A_k B_k \end{aligned} \tag{52}$$

The first and second derivatives are:

$$\begin{aligned} \frac{\mathrm{d}x_i}{\mathrm{d}\xi} &= \frac{\mathrm{d}N_a}{\mathrm{d}\xi}x_i^a \\ \frac{\mathrm{d}^2x_i}{\mathrm{d}\xi^2} &= \frac{\mathrm{d}^2N_a}{\mathrm{d}\xi^2}x_i^a \\ \frac{\mathrm{d}x_i}{\mathrm{d}\hat{\xi}} &= \frac{\mathrm{d}x_i}{\mathrm{d}\xi}\frac{\mathrm{d}\xi}{\mathrm{d}\hat{\xi}} \\ \frac{\mathrm{d}^2x_i}{\mathrm{d}\hat{\xi}^2} &= \frac{\mathrm{d}^2x_i}{\mathrm{d}\xi^2}\left(\frac{\mathrm{d}\xi}{\mathrm{d}\hat{\xi}}\right)^2 \end{aligned} \tag{53}$$

The derivative $r_{,i}$ can be expressed as

$$\begin{aligned} r_{,i} = \frac{x_i - s_i}{r} &= \frac{A_i}{A} + \left(B_iA - A_i\frac{A_kB_k}{A^3}\right)\delta + O(\delta^2) \\ &:= d_{i0} + d_{i1}\delta + O(\delta^2) \end{aligned} \tag{54}$$

The term $1/r^2$ can be expressed as

$$\begin{aligned} \frac{1}{r^2} &= \frac{1}{A^2\delta^2} - \frac{2C}{A^4\delta} + O(1) \\ &:= \frac{S_{-2}}{\delta^2} + \frac{S_{-1}}{\delta} + O(1) \end{aligned} \tag{55}$$

The component of Jacobian from parametric space to physical space can be expressed as:

$$\begin{aligned} J_1(\xi) &= J_{10}(\xi_s) + J_{11}(\xi_s)(\xi - \xi_s) + O((\xi - \xi_s)^2) \\ &= J_{10}(\xi_s) + \frac{\mathrm{d}\xi}{\mathrm{d}\hat{\xi}}\Big|_{\xi=\xi_s} J_{11}(\xi_s)\delta + O(\delta^2) \\ J_2(\xi) &= J_{20}(\xi_s) + J_{21}(\xi_s)(\xi - \xi_s) + O((\xi - \xi_s)^2) \\ &= J_{10}(\xi_s) + \frac{\mathrm{d}\xi}{\mathrm{d}\hat{\xi}}\Big|_{\xi=\xi_s} J_{21}(\xi_s)\delta + O(\delta^2) \end{aligned} \tag{56}$$

i.e.,

$$J_k(\xi) := J_{k0}(\xi_s) + \frac{\mathrm{d}\xi}{\mathrm{d}\hat{\xi}}\Big|_{\xi=\xi_s} J_{k1}(\xi_s)\delta + O(\delta^2)$$

and we note that

$$\begin{aligned} J(\xi) &= \sqrt{J_1^2(\xi) + J_2^2(\xi)} = \sqrt{\left(\frac{\mathrm{d}y}{\mathrm{d}\xi}\right)^2 + \left(-\frac{\mathrm{d}x}{\mathrm{d}\xi}\right)^2} \\ \mathbf{n}(\xi) &= \left[\frac{\mathrm{d}y}{\mathrm{d}\xi}, -\frac{\mathrm{d}x}{\mathrm{d}\xi}\right] \end{aligned} \tag{57}$$

i.e.,

$$n_k(\xi) = J_k(\xi)/J(\xi)$$

And the NURBS basis function is also expanded as:

$$\begin{aligned} N_a(\hat{\xi}) &= N_a(\hat{\xi}_s) + \frac{\mathrm{d}N_a}{\mathrm{d}\xi}\Big|_{\xi=\xi_s} (\xi - \xi_s) + \cdots \\ &= N_a(\hat{\xi}_s) + \frac{\mathrm{d}N_a}{\mathrm{d}\xi}\Big|_{\xi=\xi_s} \frac{\mathrm{d}\xi}{\mathrm{d}\hat{\xi}}\Big|_{\hat{\xi}=\hat{\xi}_s} \delta + \cdots \\ &:= N_{a0}(\hat{\xi}_s) + N_{a1}(\hat{\xi}_s) \frac{\mathrm{d}\xi}{\mathrm{d}\hat{\xi}}\Big|_{\hat{\xi}=\hat{\xi}_s} \delta + O(\delta^2) \end{aligned} \tag{58}$$

The detail form of hyper-singular kernel S_{ij} is (plane strain)

$$\begin{aligned} S_{ij}(\mathbf{s}, \mathbf{x}) = \frac{\mu}{2\pi(1-\nu)r^2} \Big\{ & 2\frac{\partial r}{\partial n} \left[(1-\nu)\delta_{ik} r_{,j} + \nu(\delta_{ij} r_{,k} + \delta_{jk} r_{,i} - 4 r_{,i} r_{,j} r_{,k})\right] \\ & + 2\nu(n_i r_{,j} r_{,k} + n_k r_{,i} r_{,j}) - (1 - 4\nu)\delta_{ik} n_j \\ & + (1 - 2\nu)(2 n_j r_{,i} r_{,k} + \delta_{ij} n_k + \delta_{jk} n_i) \Big\} n_k(\hat{\xi}_s) \\ := \frac{1}{r^2} h(\hat{\xi}) & \end{aligned} \tag{59}$$

Noting that $n_k(\xi) = J_k(\xi)/J(\xi)$, Use the above expansions to rewrite $h(\xi)$ as:

$$h(\hat{\xi}) = \frac{h_0(\hat{\xi}_s)}{J(\xi)} + \frac{h_1(\hat{\xi}_s)}{J(\xi)}\delta + O(\delta^2) \tag{60}$$

$$\begin{aligned} h_0(\hat{\xi}_s) = \Big(&2\nu(J_{i0}d_{j0}d_{k0} + J_{k0}d_{i0}d_{j0}) + (1-2\nu)(2J_{j0}d_{i0}d_{k0} + \delta_{ij}J_{k0} + \delta_{jk}J_{i0}) \\ &+ (1-4\nu)\delta_{ik}J_{j0}\Big)\frac{\mu}{2\pi(1-\nu)}n_k(\hat{\xi}_s) \end{aligned} \tag{61}$$

$$\begin{aligned} h_1(\hat{\xi}_s) = \Big[&2(d_{l1}J_{l0} + d_{l0}J_{l1})\Big((1-2\nu)\delta_{ik}d_{j0} + \nu(\delta_{ij}d_{k0} + \delta_{jk}d_{i0}) - 4d_{i0}d_{j0}d_{k0}\Big) \\ &+ 2\nu\Big(J_{i0}(d_{j1}d_{k0} + d_{j0}d_{k1}) + J_{i1}d_{j0}d_{k0} + J_{k0}(d_{i1}d_{j0} + d_{i0}d_{j1}) + J_{k1}d_{i0}d_{j0}\Big) \\ &+ (1-2\nu)\Big(2(J_{j1}d_{i0}d_{k0} + J_{j0}(d_{i1}d_{k0} + d_{i0}d_{k1})) + \delta_{ij}J_{k1} + \delta_{jk}J_{i1}\Big) \\ &- (1-4\nu)\delta_{ik}J_{j1}\Big]\frac{\mu}{2\pi(1-\nu)}n_k(\hat{\xi}_s) \end{aligned} \tag{62}$$

Thus,

$$\begin{aligned} h(\hat{\xi})N_a(\hat{\xi})J(\hat{\xi}) &= \Big(h_0(\hat{\xi}_s) + h_1(\hat{\xi}_s)\delta + O(\delta^2)\Big)\Big(N_{a0}(\hat{\xi}_s) + \frac{\mathrm{d}\xi}{\mathrm{d}\hat{\xi}}\Big|_{\hat{\xi}=\hat{\xi}_s}N_{a1}(\hat{\xi}_s)\delta + O(\delta^2)\Big) \\ &= h_0N_{a0} + (h_1N_{a0} + h_0N_{a1}\frac{\mathrm{d}\xi}{\mathrm{d}\hat{\xi}}\Big|_{\hat{\xi}=\hat{\xi}_s})\delta + O(\delta^2) \end{aligned} \tag{63}$$

$$\begin{aligned} F(\hat{\xi}_s,\hat{\xi}) &= \frac{1}{r^2(\hat{\xi}_s,\hat{\xi})}h(\hat{\xi})N_a(\hat{\xi})J(\hat{\xi}) \\ &= \Big(\frac{S_{-2}}{\delta^2} + \frac{S_{-1}}{\delta} + O(1)\Big)\Big(h_0N_{a0} + (h_1N_{a0} + h_0N_{a1}\frac{\mathrm{d}\xi}{\mathrm{d}\hat{\xi}}\Big|_{\hat{\xi}=\hat{\xi}_s})\delta + O(\delta^2)\Big) \\ &= \frac{S_{-2}h_0N_{a0}}{\delta^2} + \frac{S_{-1}h_0N_{a0} + S_{-2}(h_1N_{a0} + h_0N_{a1}\frac{\mathrm{d}\xi}{\mathrm{d}\hat{\xi}}\Big|_{\hat{\xi}=\hat{\xi}_s})}{\delta} + O(1) \\ &:= \frac{F_{-2}}{\delta^2} + \frac{F_{-1}}{\delta} + O(1) \end{aligned} \tag{64}$$

Appendix B

Once the J_1 and J_2 are evaluated properly, K_I and K_{II} can be found easily. Since

$$J_1 = \frac{K_I^2 + K_{II}^2}{E'} \tag{65a}$$

$$J_2 = -\frac{2K_IK_{II}}{E'} \tag{65b}$$

where $E' = E/(1-\nu^2)$ for plane strain condition. And K_I and K_{II} can be solved as [65]:

$$K_I = \pm\Big\{\frac{E'J_1}{2}\Big[1 \pm \Big(1 - \Big(\frac{J_2}{J_1}\Big)^2\Big)^{1/2}\Big]\Big\}^{1/2} \tag{66a}$$

$$K_{II} = \pm\Big\{\frac{E'J_1}{2}\Big[1 \mp \Big(1 - \Big(\frac{J_2}{J_1}\Big)^2\Big)^{1/2}\Big]\Big\}^{1/2} \tag{66b}$$

The signs of K_I and K_{II} correspond to the signs of crack opening displacement $[\![u_1]\!]$ and $[\![u_2]\!]$, respectively. If $[\![u_1]\!] > 0$, $K_I > 0$. The term in brace can be determined as :

$$\text{if} |[\![u_1]\!]| \geq |[\![u_2]\!]|, \text{take} + \tag{67a}$$

$$\text{if} |[\![u_1]\!]| < |[\![u_2]\!]|, \text{take} - \tag{67b}$$

Combined with Equation 65a, the following relationship can be obtained for the M integral,

$$M^{(1,2)} = \frac{2}{E'}(K_I^{(1)}K_I^{(2)} + K_{II}^{(1)}K_{II}^{(2)}) \tag{68}$$

Let state 2 be the pure mode I asymptotic fields with $K_I^{(2)} = 1$, $K_{II}^{(2)} = 0$ and K_I in real state 1 can be found as

$$K_I^{(1)} = \frac{2}{E'}M^{(1,\text{ mode } I)} \tag{69}$$

The K_{II} can be given in a similar fashion.

The auxiliary stress field $\sigma_{ij}^{(2)}$ and displacement field $u_j^{(2)}$ are given as:

$$
\begin{aligned}
\sigma_{xx} &= \frac{K_I^{(2)}}{\sqrt{2\pi r}}\cos\frac{\theta}{2}\Big(1-\sin\frac{\theta}{2}\sin\frac{3\theta}{2}\Big) - \frac{K_{II}^{(2)}}{\sqrt{2\pi r}}\sin\frac{\theta}{2}\Big(2+\cos\frac{\theta}{2}\cos\frac{3\theta}{2}\Big) \\
\sigma_{yy} &= \frac{K_I^{(2)}}{\sqrt{2\pi r}}\cos\frac{\theta}{2}\Big(1+\sin\frac{\theta}{2}\sin\frac{3\theta}{2}\Big) + \frac{K_{II}^{(2)}}{\sqrt{2\pi r}}\sin\frac{\theta}{2}\cos\frac{\theta}{2}\cos\frac{3\theta}{2} \\
\tau_{xy} &= \frac{K_I^{(2)}}{\sqrt{2\pi r}}\sin\frac{\theta}{2}\cos\frac{\theta}{2}\cos\frac{3\theta}{2} + \frac{K_{II}^{(2)}}{\sqrt{2\pi r}}\cos\frac{\theta}{2}\Big(1-\sin\frac{\theta}{2}\sin\frac{3\theta}{2}\Big) \\
u_x(r,\theta) &= \frac{K_I}{2\mu}\sqrt{\frac{r}{2\pi}}\cos\frac{\theta}{2}\left(\kappa-1+2\sin^2\frac{\theta}{2}\right) \\
&\quad + \frac{(1+\nu)K_{II}}{E}\sqrt{\frac{r}{2\pi}}\sin\frac{\theta}{2}\left(\kappa+1+2\cos^2\frac{\theta}{2}\right) \\
u_y(r,\theta) &= \frac{K_I}{2\mu}\sqrt{\frac{r}{2\pi}}\sin\frac{\theta}{2}\left(\kappa+1-2\cos^2\frac{\theta}{2}\right) \\
&\quad + \frac{(1+\nu)K_{II}}{E}\sqrt{\frac{r}{2\pi}}\cos\frac{\theta}{2}\left(1-\kappa+2\sin^2\frac{\theta}{2}\right)
\end{aligned}
\tag{70}
$$

where (r,θ) are the crack tip polar coordinates and

$$
\mu = \frac{E}{2(1+\nu)} \tag{71}
$$

$$
\kappa = \begin{cases} 3-4\nu, & \text{Plane strain} \\ (1-\nu)/(3+\nu), & \text{Plane stress} \end{cases} \tag{72}
$$

The auxiliary strain field can be obtained by differentiating u_j with respect to the physical coordinate.

References

[1] G E Blandford, A R Ingraffea, and J A Liggett. Two-dimensional stress intensity factor computations using the boundary element method. *International Journal for Numerical Methods in Engineering*, 17(3):387–404, 1981.

[2] M D Snyder and T A Cruse. Boundary-integral equation analysis of cracked anisotropic plates. *International Journal of Fracture*, 11(2):315–328, 1975.

[3] H Hong and J Chen. Derivations of Integral Equations of Elasticity. *Journal of Engineering Mechanics*, 114(6):1028–1044, 1988.

[4] A Portela, M H Aliabadi, and D P Rooke. The dual boundary element method: Effective implementation for crack problems. *International Journal for Numerical Methods in Engineering*, 33(6):1269–1287, 1992.

[5] Y Mi and M H Aliabadi. Dual boundary element method for three-dimensional fracture mechanics analysis. *Engineering Analysis with Boundary Elements*, 10(2):161–171, 1992.

[6] A P Cisilino and M H Aliabadi. Dual boundary element assessment of three-dimensional fatigue crack growth. *Engineering Analysis with Boundary Elements*, 28(9):1157–1173, 2004.

[7] A Portela. Dual boundary-element method: Simple error estimator and adaptivity. *International Journal for Numerical Methods in Engineering*, 86(12):1457–1480, 2011.

[8] S L Crouch. Solution of plane elasticity problems by the displacement discontinuity method. I. Infinite body solution. *International Journal for Numerical Methods in Engineering*, 10(2):301–343, 1976.

[9] J Dominguez and M P Ariza. A direct traction BIE approach for three-dimensional crack problems. *Engineering Analysis with Boundary Elements*, 24(10):727–738, 2000.

[10] P Partheymüller, M Haas, and G Kuhn. Comparison of the basic and the discontinuity formulation of the 3D-dual boundary element method. *Engineering Analysis with Boundary Elements*, 24(10):777–788, 2000.

[11] S Li, M E Mear, and L Xiao. Symmetric weak-form integral equation method for three-dimensional fracture analysis. *Computer Methods in Applied Mechanics and Engineering*, 151(3–4):435–459, 1998.

[12] A Frangi. Fracture propagation in 3D by the symmetric Galerkin boundary element method. *International Journal of Fracture*, 116(4):313–330, 2002.

[13] A Sutradhar and G H Paulino. Symmetric Galerkin boundary element computation of T-stress and stress intensity factors for mixed-mode cracks by the interaction integral method. *Engineering Analysis with Boundary Elements*, 28(11):1335–1350, 2004.

[14] M Bonnet, G Maier, and C Polizzoto. Symmetric Galerkin boundary element method. *Appl. Mech. Rev.*, 51:669–704, 1998.

[15] G P Nikishkov, J H Park, and S N Atluri. SGBEM-FEM alternating method for analyzing 3D non-planar cracks and their growth in structural components. *Computer Modeling in Engineering & Sciences*, 2(3):401–422, 2001.

[16] B Aour, O Rahmani, and M Nait-Abdelaziz. A coupled FEM/BEM approach and its accuracy for solving crack problems in fracture mechanics. *International Journal of Solids and Structures*, 44(7–8):2523–2539, 2007.

[17] L Dong and Atluri S N. Fracture & fatigue analyses: SGBEM-FEM or XFEM? part 2: 3D solids. *Computer Modeling in Engineering & Sciences*, 90(5):3379–3413, 2013.

[18] K M Liew, Y Cheng, and S Kitipornchai. Analyzing the 2D fracture problems via the enriched boundary element-free method. *International Journal of Solids and Structures*, 44(11–12):4220–4233, 2007.

[19] R D Henshell and K G Shaw. Crack tip finite elements are unnecessary. *International Journal for Numerical Methods in Engineering*, 9(3):495–507, 1975.

[20] Y Mi and M H Aliabadi. Discontinuous crack-tip elements: Application to 3D boundary element method. *International Journal of Fracture*, 67(3):R67–R71, 1994.

[21] J Martinez and J Dominguez. On the use of quarter-point boundary elements for stress intensity factor computations. *International Journal for Numerical Methods in Engineering*, 20(10):1941–1950, 1984.

[22] B L Karihaloo and Q Z Xiao. Accurate determination of the coefficients of elastic crack tip asymptotic field by a hybrid crack element with p-adaptivity. *Engineering Fracture Mechanics*, 68(15):1609–1630, 2001.

[23] Nader G Zamani and Weiwei Sun. A direct method for calculating the stress intensity factor in BEM. *Engineering Analysis with Boundary Elements*, 11(4):285–292, 1993.

[24] J M Melenk and I Babuška. The partition of unity finite element method: Basic theory and applications. *Computer Methods in Applied Mechanics and Engineering*, 139(1-4):289–314, 1996.

[25] N Moës, J Dolbow, and T Belytschko. A finite element method for crack growth without remeshing. *International Journal for Numerical Methods in Engineering*, 46(1):131–150, 1999.

[26] S P A Bordas, T Rabczuk, and G Zi. Three-dimensional crack initiation, propagation, branching and junction in non-linear materials by an extended meshfree method without asymptotic enrichment. *Engineering Fracture Mechanics*, 75(5):943–960, 2008.

[27] R Simpson and J Trevelyan. A partition of unity enriched dual boundary element method for accurate computations in fracture mechanics. *Computer Methods in Applied Mechanics and Engineering*, 200(1–4):1–10, 2011.

[28] M J Peake, J Trevelyan, and G Coates. Extended isogeometric boundary element method (XIBEM) for two-dimensional Helmholtz problems. *Computer Methods in Applied Mechanics and Engineering*, 259(0):93–102, 2013.

[29] M Lan, H Waisman, and I Harari. A direct analytical method to extract mixed-mode components of strain energy release rates from Irwin's integral using extended finite element method. *International Journal for Numerical Methods in Engineering*, 95(12):1033–1052, 2013.

[30] N Muthu, B G Falzon, S K Maiti, and S Khoddam. Modified crack closure integral technique for extraction of SIFs in meshfree methods. *Finite Elements in Analysis and Design*, (0):–, 2013.

[31] A Portela, M H Aliabadi, and D P Rooke. Dual boundary element analysis of cracked plates: singularity subtraction technique. *International Journal of Fracture*, 55(1):17–28, 1992.

[32] R H Rigby and M H Aliabadi. Decomposition of the mixed-mode J-integral—revisited. *International Journal of Solids and Structures*, 35(17):2073–2099, 1998.

[33] J F Yau, S S Wang, and H T Corten. A mixed-mode crack analysis of isotropic solids using conservation laws of elasticity. *Journal of Applied Mechanics*, 47:333–341, 1980.

[34] J H Chang and D J Wu. Stress intensity factor computation along a non-planar curved crack in three dimensions. *International Journal of Solids and Structures*, 44(2):371–386, 2007.

[35] K N Shivakumar and I S Raju. An equivalent domain integral method for three-dimensional mixed-mode fracture problems. *Engineering Fracture Mechanics*, 42(6):935–959, 1992.

[36] M Gosz and B Moran. An interaction energy integral method for computation of mixed-mode stress intensity factors along non-planar crack fronts in three dimensions. *Engineering Fracture Mechanics*, 69(3):299–319, 2002.

[37] T J R Hughes, J A Cottrell, and Y Bazilevs. Isogeometric analysis: CAD, finite elements, NURBS, exact geometry and mesh refinement. *Computer Methods in Applied Mechanics and Engineering*, 194(39–41):4135–4195, 2005.

[38] I Akkerman, Y Bazilevs, V M Calo, T J R Hughes, and S Hulshoff. The role of continuity in residual-based variational multiscale modeling of turbulence. *Computational Mechanics*, 41(3):371–378, 2008.

[39] Y Bazilevs, V M Calo, Y Zhang, and T J R Hughes. Isogeometric Fluid–structure Interaction Analysis with Applications to Arterial Blood Flow. *Computational Mechanics*, 38(4-5):310–322, 2006.

[40] F Auricchio, L B da Veiga, C Lovadina, and A Reali. The importance of the exact satisfaction of the incompressibility constraint in nonlinear elasticity: mixed FEMs versus NURBS-based approximations. *Computer Methods in Applied Mechanics and Engineering*, 199(5–8):314–323, 2010.

[41] D J Benson, Y Bazilevs, M C Hsu, and T J R Hughes. Isogeometric shell analysis: The Reissner–Mindlin shell. *Computer Methods in Applied Mechanics and Engineering*, 199(5–8):276–289, 2010.

[42] M J Borden, C V Verhoosel, M A Scott, T J R Hughes, and C M Landis. A phase-field description of dynamic brittle fracture. *Computer Methods in Applied Mechanics and Engineering*, 217–220(0):77–95, 2012.

[43] Y Bazilevs, V M Calo, J A Cottrell, J A Evans, T J R Hughes, S Lipton, M A Scott, and T W Sederberg. Isogeometric analysis using T-splines. *Computer Methods in Applied Mechanics and Engineering*, 199(5–8):229–263, 2010.

[44] M A Scott, X Li, T W Sederberg, and T J R Hughes. Local refinement of analysis-suitable T-splines. *Computer Methods in Applied Mechanics and Engineering*, 213–216(0):206–222, 2012.

[45] C Politis, A I Ginnis, P D Kaklis, K Belibassakis, and C Feurer. An isogeometric BEM for exterior potential-flow problems in the plane. In *2009 SIAM/ACM Joint Conference on Geometric and Physical Modeling*, SPM '09, pages 349–354, New York, NY, USA, 2009. ACM.

[46] Jinliang Gu, Jianming Zhang, and Guangyao Li. Isogeometric analysis in BIE for 3-D potential problem. *Engineering Analysis with Boundary Elements*, 36(5):858–865, 2012.

[47] R N Simpson, S P A Bordas, J Trevelyan, and T Rabczuk. A two-dimensional Isogeometric Boundary Element Method for elastostatic analysis. *Computer Methods in Applied Mechanics and Engineering*, 209–212(0):87–100, 2012.

[48] M A Scott, R N Simpson, J A Evans, S Lipton, S P A Bordas, T J R Hughes, and T W Sederberg. Isogeometric boundary element analysis using unstructured T-splines. *Computer Methods in Applied Mechanics and Engineering*, 254(0):197–221, 2013.

[49] Kang Li and Xiaoping Qian. Isogeometric analysis and shape optimization via boundary integral. *Computer-Aided Design*, 43(11):1427–1437, 2011.

[50] L Heltai, M Arroyo, and A DeSimone. Nonsingular Isogeometric Boundary Element Method for Stokes Flows in 3D. *http://dx.doi.org/10.1007/s00466-006-0084-3*, 2012.

[51] R N Simpson, M A Scott, M Taus, D C Thomas, and H Lian. Acoustic isogeometric boundary element analysis. *Computer Methods in Applied Mechanics and Engineering*, page accepted, 2013.

[52] D Arnold and J Saranen. On the Asymptotic Convergence of Spline Collocation Methods for Partial Differential Equations. *SIAM Journal on Numerical Analysis*, 21(3):459–472, 1984.

[53] P Juhl. A note on the convergence of the direct collocation boundary element method. *Journal of Sound and Vibration*, 212(4):703–719, 1998.

[54] C V Verhoosel, M A Scott, R de Borst, and T J R Hughes. An isogeometric approach to cohesive zone modeling. *International Journal for Numerical Methods in Engineering*, 87(1-5):336–360, 2011.

[55] L Piegl and W Tiller. The NURBS book. *springer*, 1995.

[56] J C F Telles. A self-adaptive co-ordinate transformation for efficient numerical evaluation of general boundary element integrals. *International Journal for Numerical Methods in Engineering*, 24(5):959–973, 1987.

[57] T J Rudolphi. The use of simple solutions in the regularization of hypersingular boundary integral equations. *Math. Comput. Model.*, 15(3-5):269–278, January 1991.

[58] Y Liu and T J Rudolphi. Some identities for fundamental solutions and their applications to weakly-singular boundary element formulations. *Engineering Analysis with Boundary Elements*, 8(6):301–311, 1991.

[59] E Lutz, A R Ingraffea, and L J Gray. Use of 'simple solutions' for boundary integral methods in elasticity and fracture analysis. *International Journal for Numerical Methods in Engineering*, 35(9):1737–1751, 1992.

[60] Y X Mukherjee, K Shah, and S Mukherjee. Thermoelastic fracture mechanics with regularized hypersingular boundary integral equations. *Engineering Analysis with Boundary Elements*, 23(1):89–96, 1999.

[61] M Tanaka, V Sladek, and J Sladeck. Regularization Techniques Applied to Boundary Element Methods. *Applied Mechanics Reviews*, 47(10):457–499, 1994.

[62] M Guiggiani, G Krishnasamy, T J Rudolphi, and F J Rizzo. A General Algorithm for the Numerical Solution of Hypersingular Boundary Integral Equations. *Journal of Applied Mechanics*, 59(3):604–614, 1992.

[63] F Auricchio, L B D Veiga, T J R Hughs, A Reali, and G Sangalli. Isogeometric collocation methods. *Mathematical Models and Methods in Applied Sciences*, 20(11):2075–2107, 2010.

[64] P A Martin and F J Rizzo. Hypersingular integrals: how smooth must the density be? *International Journal for Numerical Methods in Engineering*, 39(4):687–704, 1996.

[65] J W Eischen. An improved method for computing the J2 integral. *Engineering Fracture Mechanics*, 26(5):691–700, 1987.

[66] F Erdogan and G Sih. On the crackextension in plates under plane loading and transverse shear. *Journal of Basic Engineering*, 85:519–527, 1963.

[67] R LaGreca, M Daniel, and A Bac. Local deformation of NURBS curves. *Mathematical methods for curves and surfaces, Tromso 2004*, pages 243–252, 2005.

[68] A Paluszny and R W Zimmerman. Numerical fracture growth modeling using smooth surface geometric deformation. *Engineering Fracture Mechanics*, 108(0):19–36, 2013.

[69] H M Westergaard. Bearing pressures and cracks. *Journal of Applied Mechanics*, 6:A49–A53, 1939.

[70] D J Smith, M R Ayatollahi, and M J Pavier. The role of T-stress in brittle fracture for linear elastic materials under mixed-mode loading. *Fatigue & Fracture of Engineering Materials & Structures*, 24(2):137–150, 2001.

[71] B Cotterell and J R Rice. Slightly curved or kinked cracks. *International Journal of Fracture*, 16(2):155–169, 1980.

[72] A R Ingraffea and M Grigoriu. Probabilistic fracture mechanics: A validation of predictive capability. *Department of Structure Engineering, Cornell University*, Rep. 90-8, 1990.

[73] G Ventura, J X Xu, and T Belytschko. A vector level set method and new discontinuity approximations for crack growth by EFG. *International Journal for Numerical Methods in Engineering*, 54(6):923–944, 2002.